What is the cause(s) of large ozone variabilities in three megacity clusters in eastern China during 2015–2020?

Tingting Hu[1], Yu Lin[1], Run Liu[1,2], Yuepeng Xu[1], Shanshan Ouyang[1], Boguang Wang[1,2], Yuanhang Zhang[3], Shaw Chen Liu[1,2]

[1]Institute for Environmental and Climate Research, Jinan University, Guangzhou, 511443, China
[2]Guangdong-Hongkong-Macau Joint Laboratory of Collaborative Innovation for Environmental Quality, Guangzhou, 511443, China
[3]State Key Joint Laboratory of Environmental Simulation and Pollution Control, College of Environmental Sciences and Engineering, Peking University, Beijing, 100871, China

Correspondence to: Run Liu (liurun@jnu.edu.cn), Shaw Chen Liu (shawliu@jnu.edu.cn)

Abstract. Due to a robust emission control policy, significant reductions in major air pollutants, such as $PM_{2.5}$, SO_2, NO_2, and CO, were observed in China between 2015 to 2020. On the other hand, during the same period, there was a notable increase in ozone (O_3) concentrations, making it a prominent air pollutant in eastern China. The annual mean concentration of maximum daily 8-hour average (MDA8) O_3 exhibited alarming linear increases of 2.4, 1.1, and 2.0 ppb yr^{-1} in three megacity clusters: Beijing-Tianjin-Hebei (BTH), Yangtze River Delta (YRD) and Pearl River Delta (PRD), respectively. Meanwhile, there was a significant three-fold increase in the number of O_3-exceeding days, defined as MDA8 O_3 >75 ppb. Our analysis indicated that the upward increases in the annual mean concentration of MDA8 were primarily driven by the rise in consecutive O_3-exceeding days. There were expansions of high O_3 in urban centers to rural areas accompanied by a saturation effect that MDA8 O_3 concentrations at the high O_3 stations in 2015 remained nearly constant of 100 ppb. Lastly, we found a close association between O_3 episodes with four or more consecutive O_3-exceeding days and the position and strength of tropical cyclones (TCs) in the northwest Pacific and the West Pacific subtropical high (WPSH). The TC and WPSH contributed to meteorological conditions characterized by clear skies, subsiding air motion, high vertical stability in the lower troposphere, increased solar radiation, and positive temperature anomaly at the surface. These favorable meteorological conditions greatly facilitated the formation of O_3. Thus, we propose that the worsening O_3 increases observed in BTH, YRD and PRD from 2015 to 2020 can be mostly attributed to enhanced photochemical O_3 production resulting from an increased occurrence of meteorological conditions with high solar radiation and positive temperature anomalies under the influence of WPSH and TCs.

1 Introduction

Ozone (O_3) is an important greenhouse gas, which can also have adverse effects on human health, vegetation, and materials (Bell et al., 2006; Cohen et al., 2017; Kalabokas et al., 2020; Nuvolone et al., 2018). Surface O_3 is a secondary pollutant produced by photochemical reactions involving O_3 precursors such as volatile organic compounds (VOCs), carbon monoxide

(CO) and nitrogen oxides (NOx) (Ma et al., 2012; Monks et al., 2015; Wang et al., 2017). In addition to O_3 precursors, meteorological conditions are also crucial factors driving the O_3 formation. Solar radiation, temperature, relative humidity, wind speed, and cloud cover have been found to be closely related to O_3 formation (Dong et al., 2020; Han et al., 2020; Yin et
35   al., 2019). Furthermore, large-scale circulations, such as the East Asian monsoon, West Pacific subtropical high (WPSH) and tropical cyclones (TCs) can influence O_3 concentration as well (Lu et al., 2019; Rowlinso et al., 2019; Yang et al., 2014; Zhao and Wang, 2017).

The concentrations of air pollutants SO_2, NOx, CO, PM_{10} and $PM_{2.5}$ in China have been significantly reduced since 2013 (Li M. et al., 2021; Li et al., 2022; Zhai et al., 2019), thanks to the implementation of "Air Pollution Prevention and Control Action
40   Plan". However, the O_3 concentration has dramatically increased and emerged as a major air pollutant in eastern China (Bian et al., 2019; Fu et al., 2019; Wang et al., 2020; Zheng et al., 2018). O_3 concentrations are particularly high in the three megacity clusters in eastern China, namely Beijing-Tianjin-Hebei (BTH), Yangtze River Delta (YRD) and Pearl River Delta (PRD) (Gao et al., 2020; Guo et al., 2019; Li K. et al., 2021; Liu et al., 2018; Yang et al., 2019).

Annual mean concentrations of maximum daily 8-hour average (MDA8) O_3 in the three megacity clusters are shown in Fig. 1.
45   The linear increases of MDA8 O_3 for BTH, YRD and PRD are 2.4, 1.1 and 2.0 ppb yr^{-1}, respectively during the period 2015–2020. These increases are unusually large compared to the increases in other parts of China as well as the positive trends worldwide (Chen et al., 2020; Lu et al., 2018; Professional Committee of Ozone Pollution Control of Chinese Society for Environmental Sciences, 2022; Zhang et al., 2020). Thus, a crucial scientific question is: What is the cause(s) of these large increases in O_3 concentration? Some recent studies suggested that changing photochemical processes induced by anthropogenic
50   emissions are responsible for these increases (Li et al., 2019; Li et al., 2022; Shao et al., 2021; Wang et al., 2020). However, in our analysis of the O_3 increases at individual stations in eastern China during the period 2015–2020, we noticed that the interannual variations of O_3 concentration were strongly affected by the position and intensity of WPSH and the presence of TCs in the western Pacific and South China Sea, consistent with the results of a number of recent studies (Chang et al., 2019; Mao et al., 2020; Ouyang et al., 2022; Zhao and Wang, 2017).These results suggest that transport/meteorological parameters associated with WPSH and TCs may also play an important role in the large increases of MDA8 O_3.

The significant impact of WPSH on weather patterns and O_3 concentrations over East China is widely recognized (Bachmann, 2015; Chang et al., 2019; Yin et al., 2019; Zhao and Wang, 2017). It is well established that the WPSH plays a critical role in controlling weather conditions, which in turn affects O_3 concentrations. For example, the WPSH is known to contribute to the formation of the East Asian monsoon and influence precipitation patterns in the YRD. It also influences air temperature and
60   precipitation across North and South China (Zhang, 2001; Zhao and Wang, 2017). These changes in meteorological conditions have a profound impact on the photochemical production, dispersion, and accumulation of O_3.

Previous studies have indicated that in the peripheries of TCs, PRD experiences specific atmospheric conditions, e.g., high pressure, low humidity, and intense solar radiation, which are highly conducive to O_3 formation. These conditions often result in consecutive days with elevated levels of O_3, as observed in various case studies (Ouyang et al., 2022; Wei et al., 2016).
65   Furthermore, statistical investigations have established several noteworthy connections between TCs and O_3 concentrations in

the PRD area. For example, the meteorological conditions associated with the TC periphery frequently contributed to the formation of elevated surface O_3 levels and aerosols (Deng et al., 2019). In addition, TCs in the East China Sea had a higher likelihood of causing increased O_3 concentrations in the PRD region (Zhao et al., 2022). Lastly, TCs in the vicinity of Taiwan, China have the greatest influence on air quality in Hong Kong when compared to TCs in other areas, which is primarily because

70   these TCs facilitate the transportation of air pollutants from the PRD region (Lam et al., 2018).

In this study, we focus on exploring possible contributions to the large O_3 increases in the three megacity clusters in eastern China by changes in meteorological parameters associated with WPSH and TCs during the period 2015–2020. The rest of this paper is organized as follows. In Section 2, the data and methodology used in this study are described. Major characteristics of the O_3 interannual variability and increases in the three megacity clusters are discussed in Section 3.1. In Section 3.2, we

75   examine the spatial expansion and saturation of high O_3. The annual change of O_3-exceeding days with different durations are also examined. A hypothesis of the cause of O_3 increases in three megacity clusters in eastern China during 2015–2020 is presented in Section 3.3. Section 4 presents a summary and conclusions.

2 Data and methodology

2.1 Pollutant Data

80   The observed hourly concentrations of air pollutants, including O_3, NO_2, CO, $PM_{2.5}$, and SO_2 from 2015 to 2020 are obtained from the Chinese National Environmental Ministry of Environmental Protection (http://www.cnemc.cn/en/). Gridded MDA8 O_3 data from Tracking Air Pollution in China dataset (http://tapdata.org.cn) with a resolution of 10 km are also used (Xue et al., 2020).

2.2 Meteorological Data

85   The European Centre for Medium-Range Weather Forecasts (ECMWF) Reanalysis v5 (ERA5) dataset (available at https://cds.climate.copernicus.eu/), with a horizontal resolution of $0.25° \times 0.25°$ and a temporal resolution of 1 h, was used to analyze the influence of meteorological parameters on O_3 pollution. The variables used in this study include 2 m temperature (T2m), surface net solar radiation (SSR). In addition, daily mean relative humidity, geopotential height, zonal and meridional wind at 500 hPa, and vertical velocity at 850hPa from the National Center for Environmental Prediction (NCEP) and National

90   Center for Atmospheric Research (NCAR) reanalysis (https://psl.noaa.gov/data/gridded/data.ncep.reanalysis.html) at a resolution of $2.5° \times 2.5°$ are used.

2.3 Methods

The Chinese National Ambient Air Quality Standard for MDA8 O_3 is 160 μg m^{-3}, which corresponds to 75 ppb at 273.15 K and 1 atm. The O_3-exceeding days are defined as MDA8 O_3 concentration >75 ppb, while non-O_3-exceeding days are defined

95   as MDA8 O_3 concentration <75 ppb. According to the duration of O_3 pollution episode, it can be divided into consecutive O_3-

exceeding days with four or more days (O_3 days$\geq$4) and consecutive O_3-exceeding days less than four days (O_3 days<4). In addition, some commonly-used methods are applied in this study, including linear fitting, meteorological synthesis method, and two-tailed Student's t test.

The normalized annual mean O_3 concentration of the O_3-exceeding days is calculated by adding the O_3 concentration of the 100 O_3-exceeding day each year and dividing it by the total number of days in the year. The normalized annual mean O_3 of the non-O_3-exceeding days is calculated by the same method except for the non-O_3-exceeding days.

Table 1 lists the criteria and corresponding numbers of low O_3 and high O_3 stations in the three megacity clusters. This classification is undertaken with the purpose of distinguishing stations with various O_3 levels within the three megacity clusters, and it is based on the number of O_3 exceeding days in 2015. Stations with the number of O_3-exceeding days fewer than or 105 equal to the low O_3 criterion (second column) are considered as low O_3 stations. When more than or equal to the high O_3 criterion (4th column), they are considered as high O_3 stations. We have tested a few reasonably different criteria and found only some insignificant differences in the results. i.e., the results associated with low O_3 and high O_3 stations are robust against reasonable changes in their selection criteria. For example, the relatively large criterion (37 days) of low O_3 stations in YRD is intended to include a large enough number of stations (about one third of the total of 152 stations) to be fully representative 110 of low O_3 and moderate O_3 stations. These results have been compared to those of a more stringent criterion of nineteen days and found no notable change in the major characteristics (Figs. S1 and S2).

3 Results and discussion

3.1 Major characteristics of O_3 increases

Major characteristics of the large increases in the annual mean O_3 concentration are shown in Figs. 2a, 2b and 2c for BTH, 115 YRD and PRD, respectively, in which the normalized annual mean concentrations of MDA8 O_3 in the three megacity clusters are compared to contributions from two groups: The O_3-exceeding days and non-O_3-exceeding days. The increase in O_3-exceeding days is the primary contributor to the substantial increase in the annual mean O_3 in all three megacity clusters from 2015 to 2020. The contribution of O_3-exceeding days is affected mostly by the changing number of exceeding days (more than 80%), and secondly but nevertheless significantly by their changes in concentrations (less than 20%) (Tables 2–4). e.g., in 120 BTH the exceeding days were 31, 43, 62, 74, 96 and 78 days in the individual years of 2015–2020, respectively, while their concentrations of those years were 66.42, 64.13, 69.44, 68.21, 70.19 and 69.69, respectively (Table 2 second column). Contributions from non-O_3-exceeding days are insignificant (p-value > 0.1), except that in BTH (Fig. 2a) which shows a significant declining contribution (p-value = 0.02) due to the reduced number of non-O_3-exceeding days. Therefore, the following discussions on the O_3 increases will be focused on the O_3-exceeding days.

125 Annual numbers of single and consecutive O_3-exceeding days are shown in Figs. 3a, 3b and 3c for BTH, YRD and PRD, respectively. A drastic two to three-fold increase in the annual numbers of consecutive O_3-exceeding days can be seen in all three regions. In contrast, the numbers of single O_3-exceeding days show only a slight increase in PRD. These drastic increases

in the annual numbers of consecutive O_3-exceeding days are clearly the primary contributors to the increases in O_3 shown in Figs. 2a, 2b and 2c. This brings up two key scientific questions: What is the cause(s) of the drastic increases in the numbers of consecutive O_3-exceeding days? Is it due to changing emissions of air pollutants or changing meteorological parameters?

3.2 Spatial expansion and saturation of high O_3

Another important changing characteristics of O_3 concentrations is illustrated in Fig. 4a, which depicts the annual mean concentrations of MDA8 O_3 in BTH during O_3-exceeding days for all 78 stations (black line), 14 stations in the highest category of O_3 concentration (average 103 ppb) observed in 2015 (red line, denoted as high O_3 stations hereafter, Table 1) and 13 stations in the lowest category of O_3 (average 57 ppb) observed in 2015 (green line, denoted as low O_3 stations hereafter, Table 1). It is remarkable that O_3 concentrations at the low O_3 stations caught up within 12 ppb with other stations in merely two years (an increase of about 30 ppb from 2015 to 2017), and actually equaled the average of other stations in 2019. Meanwhile, the high O_3 stations experienced a slight decrease in O_3 concentration, albeit not statistically significant. This phenomenon suggests strongly that the annual mean concentrations of MDA8 O_3 in BTH experienced a fast (within two years) and widespread spatial expansion of high O_3 from urban centers to surrounding regions where O_3 concentrations were low in 2015. Temporally most of the expansion was accomplished during 2015–2017. This phenomenon of a fast and widespread expansion of high O_3 concentrations from urban centers to surrounding regions were also observed at a slightly less degree in YRD (Fig. 4b) and PRD (Fig. 4c).

The spatial expansion of high O_3 from urban centers to surrounding regions in BTH and YRD during 2015–2017 can be clearly visualized in Figs. 5 and 6, respectively. Figs 5a, 5b and 5c show the spatial distribution of daily mean concentrations of MDA8 O_3 for O_3-exceeding days in BTH in 2015, 2017 and their difference (2017 minus 2015), respectively. Comparing Fig. 5a to 5b, one can see that the area greater than 80-ppb (75 ppb is the O_3 exceeding standard) expanded by about a factor of five from 2015 to 2017. The daily average concentration of MDA8 O_3 within the BTH box increased from 66.42 ppb in 2015 (31 days, Fig. 5a) to 69.44 ppb in 2017 (62 days, Fig. 5b), which was a difference of 3.02 ppb or a merely 4.5% increase between the two years (Fig. 5c). After accounting for the number of O_3-exceeding days, the ratio of normalized MDA8 O_3 in all O_3-exceeding days between 2017 and 2015 became 2.09. This comparison suggests that the increase in O_3 in BTH between 2015 and 2017 was driven primarily by the increase in the number of consecutive O_3-exceeding days. Spatially Fig. 5c shows the expansion is mostly to the south and southwest outside of BTH, with YRD getting a predominant portion of O_3 enhancements. Within the BTH box, the nearly constant concentrations of O_3 inside Beijing City (40 °N, 116.5 °E) coupled with the southwestward expansion of high O_3 in 2017 (Fig. 5c) suggested that there was a saturation of O_3 inside Beijing City. There were also significant increases in O_3 in YRD and even in southern China as far as the western PRD (Fig. 5c). Nevertheless, the O_3 concentrations in YRD and PRD stayed below 70 ppb during the O_3-exceeding days of BTH in both 2015 (Fig. 5a) and 2017 (Fig. 5b). In other words, the O_3-exceeding days of YRD and PRD are mostly decoupled temporally (i.e., not occurring at the same time) from those of BTH. A logical explanation for this phenomenon is that the atmospheric conditions conducive to high O_3 formation in BTH do not overlap significantly with those conditions of YRD and PRD.

Figs. 6a, 6b and 6c are the same as Figs. 5a, 5b and 5c, respectively, but for YRD. Similar to BTH, one can clearly see the expansion of high O_3 from the vicinity of Shanghai City (31 N, 121.3 E) in the northwestern direction reaching as far as the central BTH box during the period 2015–2017 (Figs. 6b and 6c). Comparing Fig. 6a to 6b, one can see that the area greater than 70-ppb expanded from Shanghai and vicinity northwestward by more than a factor of five from 2015 to 2017. This expansion was in different direction from the southwestern expansion occurred in BTH (Fig. 5c). We note, however, this expansion does not necessarily mean the direct transport of high O_3 or its precursors from the vicinity of Shanghai to central BTH. In fact, the presence of separate rather than contiguous red patches of high O_3 (>70 ppb) in southern BTH and northern YRD in Fig. 6b is a clear indication that the high O_3 are primarily controlled by local photochemical production from local O_3 precursors, rather than the direct upwind-downwind transport of high O_3 and/or its precursors. The daily average concentration of MDA8 O_3 within the YRD box increased from 53.79 ppb in 2015 (31 days, Fig. 6a) to 64.35 ppb in 2017 (40 days, Fig. 6b), which was a difference of 10.56 ppb or a 20% increase between the two years (Fig. 6c). After accounting for the number of O_3-exceeding days, the ratio of normalized MDA8 O_3 in all O_3-exceeding days between 2017 and 2015 became 1.54. This comparison suggests that the increase in O_3 in YRD between 2015 and 2017 was due to both the increases in O_3 concentrations (+20%) and the number of O_3-exceeding days (+34%).

Figs. 7a, 7b and 7c are the same as Figs. 5a, 5b and 5c, respectively, but for PRD. Unlike BTH and YRD, there was only a slight expansion of high O_3 within the PRD box toward the southwest in 2017 compared to 2015 (Fig. 7c). Nevertheless, outside the PRD box there was an extensive expansion of high O_3 in eastern China, substantially greater than the expansion within the PRD box (Fig. 7c). The daily average concentration of MDA8 O_3 within the PRD box increased from 61.16 ppb in 2015 (14 days, Fig. 7a) to 65.18 ppb in 2017 (36 days, Fig. 7b), which was a difference of 4.02 ppb or a merely 6.6% increase between the two years (Fig. 7c). After accounting for the number of O_3-exceeding days, the ratio of normalized MDA8 O_3 in all O_3-exceeding days between 2017 and 2015 became 2.74. This comparison suggests that the increase in O_3 in PRD between 2015 and 2017 was almost entirely (93.4%) due to the increase in the number of O_3-exceeding days.

Figs 7a and 7b reconfirm that O_3-exceeding days in PRD were mostly decoupled from those in BTH (Figs. 5a and 5b) and YRD (Figs. 6a and 6b), as their spatial distributions were characterized by highly distinctive regional features in both 2015 and 2017. These differences suggest that the O_3-exceeding days mostly occur in different days in the three individual regions. On the other hand, a comparison of Figs. 7c, 6c and 5c reveals a striking common feature of high values in southwestern BTH and northwestern YRD, and low values in eastern parts of all three BTH, YRD and PRD boxes. These common features suggest that the difference between 2015 and 2017 in all three individual regions is likely caused by a common mechanism/process that changed from 2015 to 2017. Moreover, as suggested in Fig. 3, this common mechanism/process must be closely related to higher number of consecutive O_3-exceeding days in 2017 over those of 2015.

Comparison of Fig. 8a to Fig. 1 reveals an interesting point: While the yearly average MDA8 O_3 concentrations at all stations in BTH (green line in Fig 1) shows a significant O_3 increase of 2.38 ppb yr^{-1} with p=0.01, the black line in Fig. 8a (MDA8 O_3 of all stations during O_3 exceeding days) shows an insignificant increase of 1.22 ppb yr^{-1} with p=0.2. This is because the values in Fig. 8 are those of O_3 exceeding days, of which O_3 concentrations at high O_3 stations (red line in Fig. 8a) have a small

195   decrease (albeit insignificant) due to the saturation effect discussed above. This decrease is the main contributor to the high p value of 0.2 of the black line in Fig. 8a (all stations).

We believe this spatial expansion and saturation of high O_3 is a significant new finding which may provide critical clue to the cause(s) of the large O_3 increases. Its robustness against new data in 2021 and 2022 has been evaluated and reconfirmed in the Supplementary (Figure S14).

3.3 Causes of ozone enhancement at low-concentration sites and saturation at high-concentration sites

Major findings of subsections 3.1 and 3.2 can be summarized as follows: (1) Increases in O_3 observed in the three megacity clusters in eastern China during 2015–2020 (Fig. 1) were mainly caused by the large increases of approximately two to three-fold increase in the number of consecutive O_3-exceeding days (Figs. 2 and 3). (2) A fast and widespread expansion of high O_3 from urban centers to surrounding regions was observed in the three megacity clusters during 2015–2019 (Fig. 4); and the

205   majority of the expansions were accomplished during the 2015–2017 period (green lines in Fig. 4). And (3), the expansions of high O_3 in the three megacity clusters were accompanied by a saturation effect that O_3 concentrations at the high O_3 stations of approximate 100 ppb in 2015 remained nearly constant or slightly declined throughout the entire period of 2015–2020 (Fig. 4).

3.3.1 Changing emissions as a possible cause of O_3 increases in 2015–2020

210   As mentioned earlier, two emission oriented hypotheses have been proposed as a possible cause of the O_3 increases in 2015–2020. One is changing emissions of O_3 precursors NOx and VOC (Li et al., 2022). The other is the reduced removal of HO_2 radicals due to diminishing $PM_{2.5}$ (Li K. et al., 2021; Shao et al., 2021). Li et al. (2022) showed that the NO titration effect was the cause of the linear trend in O_3 in PRD (0.5 ppb yr^{-1}) during the relatively long period 2006–2019. But for the period 2015–2020, the NO titration effect could account for only about 10% of the linear increase in O_3 of the low O_3 stations in PRD (5.0

215   ppb yr^{-1}, green line, Fig.S3a).

The increase of 30 ppb in O_3 at the low O_3 stations in BTH from 2015 to 2017 (green line, Fig. 4a and Fig. 8a) represents about 50% increase in O_3. The titration effect can account for only about 5% (Fig. 8f). If this increase of 30 ppb in O_3 were due to an enhancement in O_3 precursors, the enhancement would have to be substantially greater than 50% because of the well-known less-than-linear relationship between changes in O_3 and its precursors, i.e., substantially more percentage changes in precursors

220   are needed for each percentage change in O_3 (Dodge, 1977; Shafer and Seinfeld, 1985). Figs. 8d and 8f show that CO (a proxy for VOC) and NOx changed only by a few percent from 2015 to 2017, more than one order of magnitude less than the changes needed. Hence it appears that changes in meteorological conditions conducive to O_3 formation are more likely the major contributing factor to the 50% increase in O_3 at the low O_3 stations in BTH. Similar argument can be extended to YRD and PRD (Figs. S1 and S3).

225   The theory of reduced removal of HO_2 radicals by diminishing $PM_{2.5}$ (25%, green line of Fig. 8c) appeared to be valid qualitatively for the 50% increase in O_3 at the low O_3 stations in BTH from 2015 to 2017 (green line of Fig. 8a). But this theory

was contradicted directly by the phenomenon at the high O_3 stations where a 30% reduction in $PM_{2.5}$ (red line of Fig. 8c) corresponded to a decrease rather than an increase in O_3 (red line of Fig. 8a).

3.3.2 Changes in meteorological parameters as a possible cause of O_3 increases in 2015–2020

230 Fig. 9a shows the mean daily O_3 concentrations of the first group with four or more consecutive O_3-exceeding days (labeled O_3 days$\geq$4) in 2015, Fig. 9b shows the mean daily O_3 concentrations of the second group with less than four consecutive O_3-exceeding days (labeled O_3 days<4), and Fig. 9c is the difference between the two groups (6.10 ppb, Table 2). Figs. 9d–9f are the same as Figs. 9a–9c, respectively, but for 2017. The first group in 2017 had 28 days and mean O_3 of 74.43 ppb inside the BTH box, while the second group had 34 days and 65.32 ppb (Table 2). One of the most remarkable differences between 2017

235 and 2015 in Figs. 9a–9f was the large number of days with four or more consecutive O_3-exceeding days (first group) in 2017 (28 days, Fig. 9d) over that of 2015 (7 days, Fig. 9a), which alone contributed to about 62% of the difference in O_3 between 2017 and 2015 as shown in Fig. 2a (red line). Approximately 30% was contributed by the 10 days' difference (2017 vs. 2015) in the number of days with less than four consecutive O_3-exceeding days (second group). The contribution by the higher average concentration of MDA8 O_3 of the first group in 2017 is only about 8% (Table 2). These values of contributions

240 reconfirm what is shown in Fig. 3a, i.e., the greater frequency of episodes with four or more consecutive O_3-exceeding days contributes the majority (62%) to the higher O_3 in BTH in 2017 vs. 2015, the greater intensity/concentration of O_3 during the episodes contributes only about 8%, consistent with the expansion and saturation effect discussed earlier.

The phenomena illustrated in Figs. 9a–9f also exist in YRD and PRD as well as in most other years. Figures equivalent to Figs. 9a–9c for all years in the three city clusters are provided in the Supplementary Material (Figs. S4–S6). Essential information

245 derived from those figures is summarized in Tables 2–4.

In Figs. 10a and 10b the values of SSR and T2m of the episodes with four or more consecutive O_3-exceeding days are compared to those of O_3 episodes with less than four consecutive O_3-exceeding days, and to those of clean days (non-O_3-exceeding days). As expected, the O_3 episodes with four or more consecutive O_3-exceeding days consistently have the highest values of SSR and T2m, while the clean days have the lowest values. This is the case in nearly all years studied as shown in the Supplementary

250 Material (Fig. S7) and is also generally true in YRD and PRD (Figs. S8 and S9). Coupling the higher values of SSR and T2m in the O_3 episodes with four or more consecutive O_3-exceeding days depicted in Fig. 10 and greater number of days in the O_3 episodes with four or more consecutive O_3-exceeding days shown in Fig. 3, we therefore propose a hypothesis as follows: the cause of worsening O_3 increases in BTH, YRD and PRD from 2015 to 2020 could be attributed to enhanced photochemical O_3 production due to increased occurrence of meteorological conditions of high solar radiation and positive temperature

255 anomaly at the surface.

Quantitatively the coupling of Fig. 10 with Fig. 3 can be performed by multiplying the difference between the red (four or more consecutive O_3-exceeding days) and green (clean days) values of SSR/T2m in Fig. 10 with the frequency of occurrence (in percentage of total days) of O_3 episodes with four or more consecutive O_3-exceeding days from Fig. 3. The results are compared to the yearly O_3-exceeding days in Fig. 11. Correlation between the yearly O_3-exceeding days and weighed SSR is

260 very good with R values 0.88 or greater in all three regions, lending strong support for our hypothesis. Correlation between the yearly O_3-exceeding days and weighed T2m is high correlated in BTH but not correlated in YRD and PRD, which probably suggests that T2m is not as strongly coupled to O_3 formation as SSR. Inclusion of O_3 episodes with less than four consecutive O_3-exceeding days in Fig. 11 did not change the correction coefficients significantly, supporting the robustness of results shown in Fig.11.

265 Hu W. et al. (2023), in collaboration with this study, conducted a statistical analysis to assess processes that contribute to high O_3 formation in PRD when TCs were present in the northwest Pacific. They investigated the impact of the distance between TCs in the northwest Pacific and PRD on the O_3 concentration in the PRD from 2006 to 2020. They found that the large numbers of consecutive O_3-exceeding days in 2017 and 2019 relative to 2015 were primarily attributable to the greater occurrence of downdrafts and stable atmospheric conditions brought about by mid-distance category TCs. This finding clearly

270 establishes that changing frequency of mid-distance category TCs (i.e., changing meteorological conditions) is the cause of the increases in the numbers of consecutive O_3-exceeding days as well as the higher O_3 concentrations in PRD. Ongoing study by our research group further shows that the mid-distance category TCs are predominately those TCs with tracks starting around the southern Philippines and ending near Korea and/or Japan. Since TC tracks in northwestern Pacific are strongly controlled by WPSH, we conclude that both Philippines-to-Korea/Japan track TCs and corresponding distribution and intensity of WPSH contributed to the favorable meteorological conditions leading to higher consecutive O_3-exceeding days in PRD

275 from 2015 to 2020.

Following the analysis by Hu W. et al. (2023), the mean vertical velocity at 850 hPa during all O_3-exceeding days in PRD in 2015 (Fig. 12a) is compared to that of episodes with four or more consecutive O_3-exceeding days in 2017 (Fig. 12b). Major features in Fig. 12 compare very well with those of Fig. 7. E.g., area with positive vertical velocity (downdrafts) in 2017 (red

280 area in Fig. 12b), which was highly conducive to O_3 formation, was by far more widespread and greater in value than that of 2015 (red area in Fig. 12a), agreeing well with the greater high O_3 area of Fig. 7b (2017) than that of Fig. 7a (2015). This agreement confirms that the increase in O_3 in PRD from 2015 to 2017 was caused by increased downdrafts and stable atmospheric conditions (meteorological conditions) brought about by TCs as suggested by Hu W. et al. (2023). The same plots for BTH are shown in Fig. 13. Features of Fig. 13 are highly consistent with those of Fig. 5. The same plot for YRD (Fig. S10)

285 also showed more extensive and greater downdrafts in 2017 than 2015. However, the area of positive vertical velocity in YRD appeared to shift about 500 km to the east compared to the area of high of O_3 in Fig. 6b. Considering the uncertainty in evaluating the vertical velocity and that O_3 formation is also dependent on parameters other than the vertical velocity, the discrepancy is acceptable.

In summary of this section, the increases in O_3 in the three megacity clusters are critically dependent on the number of four or

290 more consecutive O_3-exceeding days. In addition, Hu W. et al. (2023) found that the changing frequency of mid-distance category TCs (i.e., changing meteorological conditions) is the cause of the increases in the numbers of consecutive O_3-exceeding days as well as the O_3 concentrations in PRD. More importantly, our additional analyses of the mean vertical velocity at 850 hPa over the three megacity clusters (Figs. 12, 13 and S10) show that the increases in O_3 in all three megacity clusters

from 2015 to 2017 were caused by enhanced downdrafts and stable atmospheric conditions (meteorological conditions) which were highly conducive to O_3 formation. The enhanced downdrafts and stable atmospheric conditions were brought about by TCs and associated WPSH. Here we bring up WPSH because it is well known that the tracks of TCs are influenced strongly by WPSH, and that WPSH affects strongly regional atmospheric dynamics and therefore O_3 formation (Chang et al., 2019; Mao et al., 2020; Ouyang et al., 2022; Zhao and Wang, 2017).

3.3.3 Contribution of western pacific subtropical high

Mao et al. (2020) made a comprehensive study of an 11-day O_3 episode in BTH in 2017 and found it was dominated by the presence of the WPSH and mid-high latitude wave activities. Depending on the position and intensity, WPSH is well known to be a crucial factor affecting O_3 concentrations in various parts of eastern China (Chang et al., 2019; Yin et al., 2019; Zhao and Wang, 2017). During this 11-day O_3 episode, the ridge line of WPSH maintained at approximately 22 °N from June 24 to June 29, which in combination with mid-high latitude wave activities induced meteorological conditions highly conducive to the O_3 production in BTH and northern YRD (Mao et al., 2020).

Following the analysis of Mao et al. (2020), the impact of WPSH on O_3 in BTH in April–September has been analyzed in Fig. 14 which depicts the composite 500 hPa geopotential height contours, humidity and winds in BTH in April–September for O_3-exceeding days in 2015 (a), clean days in 2015 (b), O_3-exceeding days in 2017 (c), clean days in 2017 (d), O_3-exceeding days in 2019 (e) and clean days in 2019 (f). The three years 2015, 2017 and 2019 are chosen because their differences in O_3 contribute predominately to the overall O_3 increases (Figs. 1–2). The importance of WPSH is clearly visible in all Figs. 14a–14f when the 5880 and 5900 gpm isolines (green lines) of O_3-exceeding days are compared to those of clean days. In all three years, the WPSH of the former (O_3-exceeding days) were significantly stronger than the latter (clean days) as evident by the strong anticyclonic winds and/or the larger areas inside the 5880 gpm isolines. Even in the case of 2017 when the area inside 5880 gpm isolines of the former looked to be similar to that of the latter, the appearance of 5900 line in the former indicated a stronger WPSH. The strong anticyclonic winds in the O_3 exceeding days (Figs. 14a, 14c and 14e) force moist air of South China Sea northward into southern China and contributed to extensive clouds and precipitation and thus low O_3 formation over southern China and southern YRD. This difference in the O_3 formation between BTH and southern China provides a good explanation to why the O_3-exceeding days mostly occur in different time periods in the three megacity clusters as discussed in Section 3.2. Furthermore, over East China Sea the prevailing westerlies were forced northward, slowed down and lead to meteorological conditions in BTH and northern YRD characterized by cloudless sky, sinking motion and high vertical stability in the lower troposphere, as well as high SSR and positive T2m anomaly at the surface. These meteorological conditions were highly conducive to the formation and accumulation of O_3. In contrast, the weaker WPSH of the clean days allowed relatively strong westerlies to prevail over BTH during clean days in the three years, which tended to disperse O_3 (Figs. 14b, 14d and 14f). e.g., the average wind speed over BTH was about 10 m s^{-1} in Fig. 14b, while only about 5 m s^{-1} in Fig. 12a. Quantitatively Fig. 12c had 31 more O_3-exceeding days (93 ppb) than Fig. 14a, the 31 days came at the expense of clean days (52 ppb) (Figs. 14b and 14d). The contribution of these 31 days to the difference in MDA8 O_3 between 2017 and 2015 (6.5 ppb, Fig. 1) can

be calculated as follows: $((93\times62)+(56\times121))/(62+121)-((86\times31)+(52\times152))/(31+152) = 10.8$ ppb. This difference of 10.8 ppb in MDA8 O_3 between 2017 and 2015 was for the period of April to September. It should be divided by 2 and became 5.4 ppb for the yearly difference in MDA8 O_3 between 2017 and 2015. This value of 5.4 ppb accounted for 83% of the observed difference in MDA8 O_3 between 2017 and 2015 (6.5 ppb, Fig. 1). Similar statement can be made for the difference in MDA8 O_3 between 2019 and 2017 (Figs. 14e and 14c, Fig. 1).

We have made the same analysis for other years as well as for YRD and PRD. The results are mostly similar, and thus presented in the Supplementary material (Figs. S11, S12 and S13). Figs.15a–15d for PRD in 2017 and 2019 are shown because there were interesting anticyclonic circulations over PRD during O_3-exceeding days in both years (Figs. 15a and 15c). The 2017 anticyclone was a direct product of the WPSH as it resided within the western tip of the 5880 gpm isoline. The 2019 anticyclone was also likely associated with the WPSH as the center of anticyclone resided just beneath the 5860 gpm isoline to the west of PRD. The anticyclonic circulations were accompanied by stable downdrafts, low winds, and cloudless sky conditions (short arrows and blue shades in Figs. 15a and 15c), which were highly conducive to the O_3 formation. Cloudless sky conditions also occurred in YRD and BTH in Figs. 15a and 15c, but the high wind speed prevented the accumulation of O_3. This difference in O_3 accumulation between PRD and other two regions provide another good explanation to why the O_3-exceeding days mostly occur in different days in the three megacity clusters as discussed in Section 3.2. Quantitatively Fig. 15c had 27 more O_3-exceeding days (90 ppb) than Fig. 13a, the 27 days came at the expense of clean days (39 ppb) (Figs. 15b and 15d). The contribution of these 27 days to the difference in MDA8 O_3 in PRD between 2019 and 2017 (6.0 ppb, Fig. 1) can be calculated as follows: $((90\times62)+(46\times182))/(62+182)-((85\times35)+(39\times209))/(35+209)=11.6$ ppb. This difference of 11.6 ppb in MDA8 O_3 between 2019 and 2017 was for the period of April to November. It should be divided by 365/244 and became 7.75 ppb for the yearly difference in MDA8 O_3 between 2019 and 2017. This value of 7.75 ppb was 1.75 ppb more than the observed difference in MDA8 O_3 between 2019 and 2017 (6.3 ppb, Fig. 1), suggesting a reduction of about 3.5 ppb in MDA8 O_3 in the cold months of January–March and December between 2017 and 2019, which was approximately confirmed by the observed reduction of 3.88 ppb.

The presence of anticyclonic circulations over PRD is in good agreement with the results of Ouyang et al. (2022) and Hu W. et al. (2023). The latter authors suggested that the anticyclonic circulations over PRD were primarily caused by TCs in northwestern Pacific. Nevertheless, it is widely acknowledged that the tracks of TCs in the northwestern Pacific are influenced, at least to some extent, by WPSH (Sun et al., 2015; Wang et al., 2017), making it difficult to separate the roles played by the TCs on the anticyclonic circulations and O_3 formation from those of WPSH. Clearly, further investigations is needed to fully understand the complex relationship among WPSH, TCs and O_3. Based on these results, we hypothesize that the increased frequency of these meteorological conditions enabled by the changing intensity and position of WPSH could contribute as a major cause of the O_3 increases in the three megacity clusters in eastern China during 2015–2020.

3.3.4 Saturation at high-concentration sites

Why the favorable meteorological conditions only cause O_3 increase at low O_3 stations, but not at high O_3 stations? And why

360 the saturation O_3 level is around 100 ppb as shown in Fig. 4? These questions can be best addressed by examining Fig. 16 which depicts the time series of individual processes (where DDEP denotes dry deposition, CHEM the net photochemical production of O_3, HTRA the horizontal transport and VTRA the vertical transport) contributing to O_3 budget in PRD (averaged over 56 stations in PRD) calculated by the WRF-CMAQ model for the O_3 episode of September 24–October 1, 2019 (Ouyang et al., 2022). This episode was one of the most sever O_3 episodes since the official O_3 observation started in PRD in 2006.

365 MDA8 O_3 exceeded the 75 ppb standard on all eight days of the episode. Hourly O_3 reached as high as 110 ppb, yet all MDA8 O_3 stayed approximately between 75 and 100 ppb. This suggests a ceiling/saturation level of approximately 100 ppb for MDA8 O_3, consistent with what was observed in Fig. 4 for PRD as well as BTH and YRD. Since this episode was one of the most sever episodes, we can assume that the 100 ppb saturation level would also be applicable to other O_3 episodes in Guangdong. More importantly, the saturation effect was also a common feature in the results of other three-dimensional models for other

370 megacity clusters, in which MDA8 O_3 usually saturated at 100 ppb, e.g., in YRD (Li et al., 2012) and in Beijing (Zhang et al., 2023). This explains why the saturation O_3 level is around 100 ppb as shown in Fig. 4.

In regard to the first question: Why the favorable meteorological conditions only cause O_3 increase at low O_3 stations, but not at high O_3 stations? It can be understood as follows: At a low O_3 station of 65 ppb MDA8 O_3 in PRD in 2015 (Fig. 4c), Fig. 16 shows that MDA8 O_3 can readily increase to 75–100 ppb in a few hours from an early morning low ozone of about 50 ppb

375 under favorable meteorological conditions. However, at a high O_3 station of 100 ppb MDA8 O_3 in 2015 (Fig. 4c) under the same favorable meteorological conditions, MDA8 O_3 would also reach 75–100 ppb in a few hours from an early morning low ozone of about 50 ppb (Note here we assume all stations start the day with an early morning low ozone of 50 ppb, consistent with the value in Fig. 16). In other words, the saturation levels at all stations are the same at 75–100 ppb, independent of the ozone concentration in 2015.

380 In terms of contributing processes, the saturation level of 75–100 ppb is controlled primarily by photochemical loss, dry deposition and dispersion to the free troposphere. This can be clearly seen in Fig. 16, on all eight days in the mid-morning when O_3 is approaching toward its peak value, CHEM declines sharply due to photochemical loss, and HTRA, VTRA and DDEP all become greater. Near noontime O_3 starts to drop sharply.

3.4 Uncertainty and cautionary statements

385 It is worth noting that the analyses conducted in Sections 3.1–3.3 have predominantly relied on correlation or regression analysis techniques, which do not imply a cause-and-effect relationship. To establish a cause-and-effect link between the proposed changes in meteorological parameters and O_3 increases, it is necessary to employ a mechanistic model that is based on the proposed causes and can accurately reproduce the observed O_3 increase. Until such model reproduction is achieved, all correlation or regression findings should be considered as a potential maximum cause-and-effect relationship (Wu et al., 2022).

390 However, current mechanistic models suffer from significant uncertainties, making it difficult to credibly simulate critical

atmospheric processes that regulate O_3 formation. These processes include atmospheric transport parameterizations, the sources and sinks of OH, HO_2 and RO_2 radicals, and the photochemistry of VOCs and OVOCs.

4 Summary and Conclusions

Thanks to a strong emission control policy, major air pollutants in China, including $PM_{2.5}$, SO_2, NO_2 and CO had shown remarkable reductions during 2015–2020. However, O_3 concentration had increased significantly and emerged as a major air pollutant in eastern China during the same time period. The annual mean concentration of MDA8 in three megacity clusters in eastern China, namely BTH, YRD and PRD, showed alarming large upward linear increases of 25%, 10% and 19%, respectively during 2015–2019. Identifying the causes of these worsening O_3 increases is urgently required for air pollution prevention and management. Some recent studies suggested that enhanced photochemical processes induced by changing anthropogenic emissions were responsible for these increases (Li et al., 2019; Li et al., 2022; Shao et al., 2021; Wang et al., 2020). However, we noticed that there were independent pieces of evidence, including the spatial expansion of high O_3 (Figs. 5 and 6) and inter-annual variations in O_3, Ox, NO_2, CO and $PM_{2.5}$ (Fig. 8), suggesting that transport/meteorological conditions rather than emissions of O_3 precursors were more likely to be the major contributor to the O_3 increases. Moreover, we found that the increases in O_3 observed in the three megacity clusters during 2015–2020 (Fig. 1) were mainly caused by the approximately two to three-fold increase in the number of consecutive O_3-exceeding days (Fig. 3). In addition, there was a fast and widespread expansion of high O_3 from urban centers to surrounding regions (Fig. 4), and most of the expansions was accomplished during the 2015–2017 period (green lines in Fig. 4). Furthermore, the expansions of high O_3 in the three megacity clusters were accompanied by a saturation effect, of that the O_3 concentrations at high O_3 stations in 2015 of approximate 100 ppb remained nearly constant throughout 2015–2022 (Fig. S14), while the low O_3 stations in 2015 with O_3 less than 75 ppb in all three megacity clusters experienced a significant enhancement in O_3 (>5 ppb yr^{-1}) during 2015–2017 (Figs. 4a, 4b and 4c). Finally, greater frequency of episodes with four or more consecutive O_3-exceeding days contributed to the majority of the increases in O_3 in all three megacity clusters in between 2015 and 2017.

Coupling the higher values of SSR and T2m in the O_3 episodes with four or more consecutive O_3-exceeding days depicted in Fig. 10 and greater occurrence (number of days) in the O_3 episodes with four or more consecutive O_3-exceeding days shown in Fig. 3, we hypothesize that the cause of the worsening O_3 increases in BTH, YRD and PRD from 2015 to 2020 could be attributed to enhanced photochemical O_3 production due to the increased occurrence of meteorological conditions of high solar radiation and positive temperature anomaly under the influence of WPSH and TCs. The hypothesis is substantiated in Fig. 11, which shows excellent correlation between the yearly O_3-exceeding days and SSR with R values 0.88 or greater in all three regions. Correlation between the yearly O_3-exceeding days and T2m is good in BTH but poor in YRD and PRD, which probably suggests that T2m is not as strongly coupled to O_3 formation as SSR.

The increases in O_3 in the three megacity clusters are found to be critically dependent on the number of four or more consecutive O_3-exceeding days. In collaboration with this study, Hu W. et al. (2023) found that the changing frequency of

mid-distance category TCs (i.e., changing meteorological conditions) is the cause of the increases in the numbers of consecutive O_3-exceeding days as well as the O_3 concentrations in PRD. Our additional analyses of the mean vertical velocity at 850 hPa in the three megacity clusters (Figs. 12, 13 and S10) show that the increases in O_3 in all three megacity clusters from 2015 to 2017 were associated with enhanced downdrafts and stable atmospheric conditions (meteorological conditions) which were highly conducive to O_3 formation. Finally, the enhanced downdrafts and stable atmospheric conditions were most likely brought about by TCs and associated WPSH.

Therefore, we propose that the O_3 concentrations at the high O_3 stations stayed close to a saturation level of about 100 ppb throughout 2015 to 2020, even under more frequent conditions conducive to O_3 formation, was the result of a relatively high rates of atmospheric dispersion, dry deposition and photochemical loss due to the high O_3 concentration (Fig. 16). While the low O_3 stations, where O_3 production were relatively small in 2015, experienced significant enhancements in the O_3 production in 2017 and 2019 because of more frequent downdrafts and stable atmospheric conditions associated with TCs and WPSH in the northwestern Pacific, which were highly conducive to O_3 photochemical production and accumulation (Hu W. et al., 2023). Following the analysis of Mao et al. (2020), the impact of WPSH on O_3 in BTH in April–September has been analyzed in Fig. 14. We found that the increased frequency of these meteorological conditions enabled by the changing intensity and position of WPSH could contribute as a major cause of the O_3 increases in the three megacity clusters in eastern China during 2015–2020.

Nevertheless, it is crucial to recognize that the examinations carried out in Sections 3.1–3.3 primarily utilized correlation or regression analysis techniques, which do not inherently establish causal relationships. To attribute cause and effect between the suggested alterations in meteorological parameters and O_3 increases, it is necessary to employ a mechanistic model that accurately replicates the observed O_3 increase based on the proposed cause(s). Until the model successfully reproduces the phenomenon, all correlation or regression findings should be treated as merely indicating the highest potential cause-and-effect relationship (Wu et al., 2022).

In conclusion, we hypothesize that the cause of the worsening O_3 increases in BTH, YRD and PRD from 2015 to 2020 is attributable to enhanced photochemical O_3 production due to the increased occurrence of meteorological conditions of high solar radiation and positive temperature anomaly under the influence of WPSH and TCs. Therefore, we suggest that future O_3 pollution prevention and control policies should pay more attention to changes in the meteorological/climate conditions, particularly changes in the large-scale circulations, including WPSH and TCs.

Data availability. Hourly surface O_3, NO_2, CO, $PM_{2.5}$, and SO_2 data were obtained from China National Environmental Centre (http://www.cnemc.cn/en/). Hourly meteorological data are obtained from European Centre for Medium-Range Weather Forecasts ERA5 reanalysis (https://cds.climate.copernicus.eu/). Daily meteorological data are obtained from National Center for Environmental Prediction (NCEP) and National Center for Atmospheric Research (NCAR) (https://psl.noaa.gov/data/gridded/data.ncep.reanalysis.html). The data of this study are available upon request to Shaw Chen Liu (shawliu@jnu.edu.cn).

Author Contributions. SL and RL proposed the essential research idea. TH, and YL performed the analysis. TH, YL, RL, and SL drafted the manuscript. YX, SO, BW, and YZ helped analysis and offered valuable comments. All authors have read and agreed to the published version of the manuscript.

Competing interests. The authors declare that they have no conflict of interest.

Acknowledgments. The authors thank the China National Environmental Centre and European Centre for Medium-Range Weather Forecasts for providing datasets that made this work possible. We also acknowledge the support of the Institute for Environmental and Climate Research and Guangdong-Hongkong-Macau Joint Laboratory of Collaborative Innovation for Environmental Quality in Jinan University.

Financial support. This research was supported by the National Natural Science Foundation of China (grant number 92044302, 41805115), Guangzhou Municipal Science and Technology Project, China (grant number 202002020065), Special Fund Project for Science and Technology Innovation Strategy of Guangdong Province (grant number 2019B121205004), Guangdong Innovative and Entrepreneurial Research Team Program (grant number 2016ZT06N263), and National Key Research and Development Program of China (grant number 2018YFC0213906).

References

Bachmann, J. D.: Air quality and climate connections, J. Air Waste Manage., 65, 641–644, https://doi.org/10.1080/10962247.2015.1040697, 2015.

Bell, M. L., Peng, R. D., and Dominci, F.: The exposure–response curve for ozone and risk of mortality and the adequacy of current ozone regulations, Environ. Health Perspect., 114, 532–536, https://doi.org/10.1289/ehp.8816, 2006.

Bian, Y., Huang, Z., Ou, J., Zhong, Z., Xu, Y., Zhang, Z., Xiao, X., Ye, X., Wu, Y., Yin, X., Li, C., Chen, L., Shao, M., and Zheng, J.: Evolution of anthropogenic air pollutant emissions in Guangdong Province, China, from 2006 to 2015, Atmos. Chem. Phys., 19, 11701–11719, https://doi.org/10.5194/acp-19-11701-2019, 2019.

Chang, L., Xu, J., Tie, X., and Gao, W.: The impact of Climate Change on the Western Pacific Subtropical High and the related ozone pollution in Shanghai, China, Sci. Rep., 9, 16998, https://doi.org/10.1038/s41598-019-53103-7, 2019.

Chen, Z., Li, R., Chen, D., Zhuang, Y., Gao, B., Yang, L., and Li, M.: Understanding the causal influence of major meteorological factors on ground ozone concentrations across China, J. Clean. Prod., 242, 118498, https://doi.org/10.1016/j.jclepro.2019.118498, 2020.

Cohen, A. J., Brauer, M., Burnett, R., Anderson, H. R., Frostad, J., Estep, K., Balakrishnan, K., Brunekreef, B., Dandona, L., Dandona, R., Feigin, V., Freedman, G., Hubbell, B., Jobling, A., Kan, H., Knibbs, L., Liu, Y., Martin, R., Morawska, L., Pope III C. A., Shin, H., Straif, K., Shaddick, G., Thomas, M., van Dingenen, R., van Donkelaar, A., Vos, T., Murray, C. J. L., and Forouzanfar, M. H.: Estimates and 25-year trends of the global burden of disease attributable to ambient air pollution: an analysis of data from the Global Burden of Diseases Study 2015, The Lancet, 389, 1907–1918, https://doi.org/10.1016/S0140-6736(17)30505-6, 2017.

Deng, T., Wang, T., Wang, S., Zou, Y., Yin, C., Li, F., Liu, L., Wang, N., Song, L., Wu, C., and Wu, D.: Impact of typhoon periphery on high ozone and high aerosol pollution in the Pearl River Delta region, Sci. Total Environ., 668, 617–630, https://doi.org/10.1016/j.scitotenv.2019.02.450, 2019.

Dodge, M. C.: Effect of selected parameters on predictions of a photochemical model, PB-269858; EPA-600/3-77/048, Environmental Protection Agency, Research Triangle Park, N. C., U.S.A., 1977.

Dong, Y., Li, J., Guo, J., Jiang, Z., Chu, Y., Chang, L., Yang, Y., and Liao, H.: The impact of synoptic patterns on summertime ozone pollution in the North China Plain, Sci. Total Environ., 735, 139559, https://doi.org/10.1016/j.scitotenv.2020.139559, 2020.

Fu, Y., Liao, H., and Yang, Y.: Interannual and decadal changes in tropospheric ozone in China and the associated chemistry-climate interactions: a review, Adv. Atmos. Sci., 36, 975–993, https://doi.org/10.1007/s00376-019-8216-9, 2019.

Gao, D., Xie, M., Chen, X., Wang, T., Liu, J., Xu, Q., Mu, X., Chen, F., Li, S., Zhuang, B., Li, M., Zhao, M., and Ren, J.: Systematic classification of circulation patterns and integrated analysis of their effects on different ozone pollution levels in the Yangtze River Delta Region, China. Atmos. Environ., 242, 117760, https://doi.org/10.1016/j.atmosenv.2020.117760, 2020.

Guo, H., Chen, K., Wang, P., Hu, J., Ying, Q., Gao, A., and Zhang, H.: Simulation of summer ozone and its sensitivity to emission changes in China, Atmos. Pollut. Res., 10, 543–1552, https://doi.org/10.1016/j.apr.2019.05.003, 2019.

Han, H., Liu, J., Shu, L., Wang, T., and Yuan, H.: Local and synoptic meteorological influences on daily variability in
510   summertime surface ozone in eastern China, Atmos. Chem. Physics., 20, 203–222. https://doi.org/10.5194/acp-20-203-2020, 2020.

Hu, W., Liu, R., Chen, Z., Ouyang, S., Hu, T., Wang, Y., Cui, Z., Jiang, B., Chen, D., Liu, S.C., Processes conducive to high ozone formation in Pearl River Delta in the presence of Pacific tropical cyclones, Atoms. Environ., 307, 119859, https://doi.org/10.1016/j.atmosenv.2023.119859, 2023.

515   Kalabokas, P., Jensen, N.R., Roveri, M., Hjorth, J., Eremenko, M., Cuesta, J., Dufour, G., Foret, G., Beekmann, M.: A study of the influence of tropospheric subsidence on spring and summer surface ozone concentrations at the JRC Ispra station in northern Italy, Atmos. Chem. Phys., 20, 1861–1885, https://doi.org/10.5194/acp-20-1861-2020, 2020.

Lam, Y. F., Cheung, H. M., and Ying, C. C.: Impact of tropical cyclone track change on regional air quality, Sci. Total Environ., 610–611, 1347–1355, https://doi.org/10.1016/j.scitotenv.2017.08.100, 2018.

520   Li, K., Jacob, D. J., Liao, H., Shen, L., Zhang, Q., and Bates, K. H.: Anthropogenic drivers of 2013–2017 trends in summer surface ozone in China, Proc. Natl. Acad. Sci. U.S.A., 116, 422–427, https://doi.org/10.1073/pnas.181216811, 2019.

Li, K., Jacob, D. J., Liao, H., Qiu, Y., Shen, L., Zhai, S., Bates, K. H., Sulprizio, M. P., Song, S., Lu, X., Zhang, Q., Zheng, B., Zhang, Y., Lee, H. C., and Su, K. K.: Ozone pollution in the North China Plain spreading into the late-winter haze season, Natl. Acad. Sci. U.S.A., 118, e2015797118, https://doi.org/10.1073/pnas.2015797118, 2021.

525   Li, L., Chen, C. H., Huang, C., Huang, H. Y., Zhang, G. F., Wang, Y. J., Wang, H. L., Lou, S. R., Qiao, L. P., Zhou, M., Chen, M. H., Chen, Y. R., Streets, D. G., Fu, J. S., and Jang, C. J.: Process analysis of regional ozone formation over the Yangtze River Delta, China using the Community Multi-Scale Air Quality modeling system, Atmos. Chem. Phys., 12, 10791–10987. https://doi.org/10.5194/acp-12-10971-2012, 2012.

Li, M., Wang, T., Shu, L., Qu, Y., Xie, M., Liu, J., Wu, H., Kalsoom, U.: Rising surface ozone in China from 2013 to 2017:
530   A response to the recent atmospheric warming or pollutant controls? Atmos. Environ., 246, 118130, https://doi.org/10.1016/j.atmosenv.2020.118130, 2021.

Li, X., Yuan, B., Parrish, D. D., Chen, D., Song, Y., Yang, S., Liu, Z., Shao, M.: Long-term trend of ozone in southern China reveals future mitigation strategy for air pollution, Atmos. Environ., 269, 118869, https://doi.org/10.1016/j.atmosenv.2021.118869, 2022.

535   Liu, H., Liu, S., Xue, B., Lv, Z., Meng, Z., Yang, X., Xue, T., Yu, Q., and He, K.: Ground-level ozone pollution and its health impacts in China, Atmos. Environ., 173, 223–230, https://doi.org/10.1016/j.atmosenv.2017.11.014, 2018.

Lu, X., Hong, J., Zhang, L., Cooper, O. R., Schultz, M. G., Xu, X., Wang, T., Gao, M., Zhao, Y., and Zhang, Y.: Severe surface ozone pollution in China: A global perspective, Environ. Sci. Technol. Lett., 5, 487–494, https://doi.org/10.1021/ACS.ESTLETT.8B00366, 2018.

540 Lu, X., Zhang, L., and Shen, L.: Meteorology and climate influences on tropospheric ozone: a review of natural sources, chemistry, and transport patterns, Curr. Pollution Rep., 5, 238–260, https://doi.org/10.1007/s40726-019-00118-3, 2019.

Ma, J., Xu, X., Zhao, C., and Yan, P.: A review of atmospheric chemistry research in China: Photochemical smog, haze pollution, and gas-aerosol interactions, Adv. Atmos. Sci., 29, 1006–1026, https://doi.org/10.1007/s00376-012-1188-7, 2012.

Mao, J., Wang, L., Lu, C., Liu, J., Li, M., Tang, G., Ji, D., Zhang, N., and Wang, Y.: Meteorological mechanism for a large-

545 scale persistent severe ozone pollution event over eastern China in 2017, J. Environ. Sci., 92, 187–199, https://doi.org/10.1016/j.jes.2020.02.019, 2020.

Monks, P. S., Archibald, A. T., Colette, A., Cooper, O., Coyle, M., Derwent, R., Fowler, D., Granier, C., Law, K. S., Mills, G. E., Stevenson, D. S., Tarasova, O., Thouret, V., von Schneidemesser, E., Sommariva, R., Wild, O., and Williams, M. L.: Tropospheric ozone and its precursors from the urban to the global scale from air quality to short-lived climate forcer, Atmos.

550 Chem. Phys., 15, 8889–8973, https://doi.org/10.5194/acp-15-8889-2015, 2015.

Nuvolone, D., Petri, D., and Voller, F.: The effects of ozone on human health, Environ. Sci. Pollut. Res. Int., 25, 8074–8088, https://doi.org/10.1007/s11356-017-9239-3, 2018.

Ouyang, S., Deng, T., Liu, R., Chen, J., He, G., Leung, J. C.-H., Wang, N., and Liu, S. C.: Impact of a subtropical high and a typhoon on a severe ozone pollution episode in the Pearl River Delta, China, Atmos. Chem. Phys., 22, 10751–10767,

555 https://doi.org/10.5194/acp-22-10751-2022, 2022.

Professional Committee of Ozone Pollution Control of Chinese Society for Environmental Sciences: The Bluebook: Prevention and Control of Ozone Pollution in China (2020), Science Press, Beijing, China, ISBN 978-7-03-071664-4, 2022 (in Chinese).

Rowlinson, M. J., Rap, A., Arnold, S. R., Pope, R. J., Chipperfield, M. P., McNorton, J., Forster, P., Gordon, H., Pringle, K. J., Feng, W., Kerridge, B. J., Latter, B. L., and Siddans, R.: Impact of El Niño–Southern Oscillation on the interannual

560 variability of methane and tropospheric ozone, Atmos. Chem. Phys., 19, 8669–8686, https://doi.org/10.5194/acp-19-8669-2019, 2019.

Shafer, T. B., and Seinfeld, J. H.: Evaluation of chemical reaction mechanisms for photochemical smog. Part 3. Sensitivity of EKMA (Empirical Kinetic Modeling Approach) to chemical mechanism and input parameters. Final Report, March 1984– February 1985, PB-85-210888/XAB, California Institute of Technology, Pasadena, U.S.A., 1985.

565 Shao, M., Wang, W., Yuan, B., Parrish, D. D., Li, X., Lu, K., Wu, L., Wang, X., Mo, Z., Yang, S., Peng, Y., Kuang, Y., Chen, W., Hu, M., Zeng, L., Su, H., Cheng, Y., Zheng, J., and Zhang, Y.: Quantifying the role of $PM_{2.5}$ dropping in variations of ground-level ozone: Inter-comparison between Beijing and Los Angeles, Sci. Total Environ., 788, 147712, https://doi.org/10.1016/j.scitotenv.2021.147712, 2021.

Sun, Y., Zhong, Z., Yi, L., Li, T., Chen, M., Wan, H., Wang, Y., and Zhong, K.: Dependence of the relationship between the

570 tropical cyclone track and western Pacific subtropical high intensity on initial storm size: A numerical investigation. J. Geophys. Res. Atmos., 120(22), 11451–11467, https://doi.org/10.1002/2015jd023716, 2015.

Wang, T., Xue, L., Brimblecombe, P., Lam, Y. F., Li, L., and Zhang, L.: Ozone pollution in China: A review of concentrations, meteorological influences, chemical precursors, and effects, Sci. Total Environ., 575, 1582–1596, https://doi.org/10.1016/j.scitotenv.2016.10.081, 2017.

575   Wang, Y., Gao, W., Wang, S., Song, T., Gong, Z., Ji, D., Wang, L., Liu, Z., Tang, G., Huo, Y., Tian, S., Li, J., Li, M., Yang, Y., Chu, B., Petäjä, T., Kerminen, V.-M., He, H., Hao, J., Kulmala, M., Wang, Y., and Zhang, Y.: Contrasting trends of $PM_{2.5}$ and surface-ozone concentrations in China from 2013 to 2017, Natl. Sci. Rev., 7, 1331–1339, https://doi.org/10.1093/nsr/nwaa032, 2020.

Wei, X., Lam, K.-S., Cao, C., Li, H., and He, J.: Dynamics of the Typhoon Haitang related high ozone episode over Hong

580   Kong, Adv. Meteorol., 6089154, https://doi.org/10.1155/2016/6089154, 2016.

Wu, Y., Liu, R., Li, Y., Dong, J., Huang, Z., Zheng, J., and Liu. S. C.: Contributions of meteorology and anthropogenic emissions to the trends in winter $PM_{2.5}$ in eastern China 2013–2018, Atmos. Chem. Phys., 22, 11945–11955, https://doi.org/10.5194/acp-22-11945-2022, 2022.

Xue, T., Zheng, Y., Geng, G., Xiao, Q., Meng, X., Wang, M., Li, X., Wu, N., Zhang, Q., and Zhu, T.: Estimating spatiotemporal

585   variation in ambient ozone exposure during 2013–2017 using a data-fusion model, Environ. Sci. Technol., 54, 14877–14888, https://doi.org/10.1021/acs.est.0c03098, 2020.

Yang, W., Chen, H., Wang, W., Wu, J., Li, J., Wang, Z., Zheng, J., and Chen, D.: Modeling study of ozone source apportionment over the Pearl River Delta in 2015, Environ. Pollut., 253, 393–402, https://doi.org/10.1016/j.envpol.2019.06.091, 2019.

590   Yang, Y., Liao, H., and Li, J.: Impacts of the East Asian summer monsoon on interannual variations of summertime surface-layer ozone concentrations over China, Atmos. Chem. Phys., 14, 6867–6879, https://doi.org/10.5194/acp-14-6867-2014, 2014.

Yin, Z., Cao, B., and Wang, H.: Dominant patterns of summer ozone pollution in eastern China and associated atmospheric circulations, Atmos. Chem. Phys., 19, 13933–13943, https://doi.org/10.5194/acp-19-13933-2019, 2019.

Zhai, S., Jacob, D. J., Wang, X., Shen, L., Li, K., Zhang, Y., Gui, K., Zhao, T., and Liao, H.: Fine particulate matter ($PM_{2.5}$)

595   trends in China, 2013–2018: separating contributions from anthropogenic emissions and meteorology, Atmos. Chem. Phys., 19, 11031– 11041, https://doi.org/10.5194/acp-19-11031-2019, 2019.

Zhang, Y., Tao, M., Zhang, J., Liu, Y., Chen, H., Cai, Z., and Konopka, P.: Long-term variations in ozone levels in the troposphere and lower stratosphere over Beijing: observations and model simulations, Atmos. Chem. Phys., 20, 13343–13354, https://doi.org/10.5194/acp-20-13343-2020, 2020.

600   Zhang, R.: Relations of water vapor transport from Indian Monsoon with that over East Asia and the summer rainfall in China. Adv. Atmos. Sci. 18 (5), 1005–1017, http://doi.org/10.1007/bf03403519, 2001.

Zhang, S., Zhang, Z., Li, Y., Du, X., Qu, L., Tang, W., Xu, J. and Meng, F.: Formation processes and source contributions of ground-level ozone in urban and suburban Beijing using the WRF-CMAQ modelling system, J. Environ. Sci., 127, 753–766, https://doi.org/10.1016/j.jes.2022.06.016, 2023.

605   Zhao, W., LÜ, M., Lu, Q., Gao, B., Liang, X., Liu, M., Sun, J., Chen, L., and Fan, S.: Effects of tropical cyclones on ozone pollution in the Pearl River Delta in autumn, Environ. Sci., 43, 2957–2965, https://doi.org/10.13227/j.hjkx.202109169, 2022 (in Chinese).

Zhao, Z. and Wang, Y.: Influence of the West Pacific subtropical high on surface ozone daily variability in summertime over eastern China, Atmos. Environ., 170, 197–204, https://doi.org/10.1016/j.atmosenv.2017.09.024, 2017.

610   Zheng, B., Tong, D., Li, M., Liu, F., Hong, C., Geng, G., Li, H., Li, X., Peng, L., Qi, J., Yan, L., Zhang, Y., Zhao, H., Zheng, Y., He, K., and Zhang, Q.: Trends in China's anthropogenic emissions since 2010 as the consequence of clean air actions, Atmos. Chem. Phys., 18, 14095–14111, https://doi.org/10.5194/acp-18-14095-2018, 2018.

Table 1. Criteria and corresponding numbers of low O_3 and high O_3 stations in the three megacity clusters in 2015. The criterion listed for each megacity cluster was based on the number of MDA8 O_3 exceeding days in 2015. For instance, the criterion for 615   a low O_3 site in BTH was the number of MDA8 O_3 exceeding days in 2015 being less than or equal to 19 days, while for high O_3 site was the number of MDA8 O_3 exceeding days in 2015 being greater than or equal to 71 days.

	Criterion of low O_3 stations	Number of low O_3 stations	Criterion of high O_3 stations	Number of high O_3 stations	Total number of stations
BTH	≤ 19 days	13	≥ 71 days	14	78
YRD	≤ 37 days	54	≥ 67 days	13	152
PRD	≤ 12 days	10	≥ 46 days	10	48

Table 2. Mean O_3 concentrations (ppb) and number of days of all O_3-exceeding days (2nd column), consecutive O_3-exceeding days with less than four days (3rd column), consecutive O_3-exceeding days with four or more days (4th column) and the difference between ($\geq$4days) and (<4days) (5th column) within the BTH box in 2015–2020.

	All days Concentration (days) ppb	<4 days Concentration (days) ppb	$\geq$4 days Concentration (days) ppb	Difference ($\geq$4 days) – (<4 days) ppb
2015	66.42(31)	65.04(24)	71.14(07)	6.10
2016	64.13(43)	62.65(26)	66.39(17)	3.74
2017	69.44(62)	65.32(34)	74.43(28)	9.11
2018	68.21(74)	65.43(27)	69.80(47)	4.37
2019	70.19(96)	65.28(30)	72.42(66)	7.14
2020	69.69(78)	65.52(40)	74.08(38)	8.56

Table 3. Mean O_3 concentrations (ppb) and number of days of all O_3-exceeding days (2nd column), consecutive O_3-exceeding days with less than four days (3rd column), consecutive O_3-exceeding days with four or more days (4th column) and the difference between ($\geq$4days) and ($<$4days) (5th column) within the YRD box in 2015–2020.

	All days	<4 days	≥4 days	Difference
	Concentration (days) ppb	Concentration (days) ppb	Concentration (days) ppb	(≥4 days) – (<4 days) ppb
2015	53.79(31)	53.59(19)	54.11(12)	0.52
2016	58.87(27)	58.03(23)	63.73(04)	5.70
2017	64.35(40)	62.62(25)	67.22(15)	4.60
2018	63.33(43)	62.49(32)	65.75(11)	3.26
2019	67.18(49)	66.09(27)	68.51(22)	2.42
2020	65.84(38)	64.12(27)	70.06(11)	5.94

625

Table 4. Mean O_3 concentrations (ppb) and number of days of all O_3-exceeding days (2nd column), consecutive O_3-exceeding days with less than four days (3rd column), consecutive O_3-exceeding days with four or more days (4th column) and the difference between ($\geq$4days) and (<4days) (5th column) within the PRD box in 2015–2020.

	All days	<4 days	$\geq$4 days	Difference
	Concentration (days) ppb	Concentration (days) ppb	Concentration (days) ppb	($\geq$4 days) – (<4 days) ppb
2015	61.16(14)	61.16(14)	---(0)	---
2016	58.44(19)	58.44(19)	---(0)	---
2017	65.18(36)	64.60(23)	66.20(13)	1.60
2018	65.82(31)	63.27(16)	68.55(15)	5.28
2019	69.80(62)	65.96(29)	73.16(33)	7.20
2020	65.08(37)	63.87(22)	66.84(15)	2.97
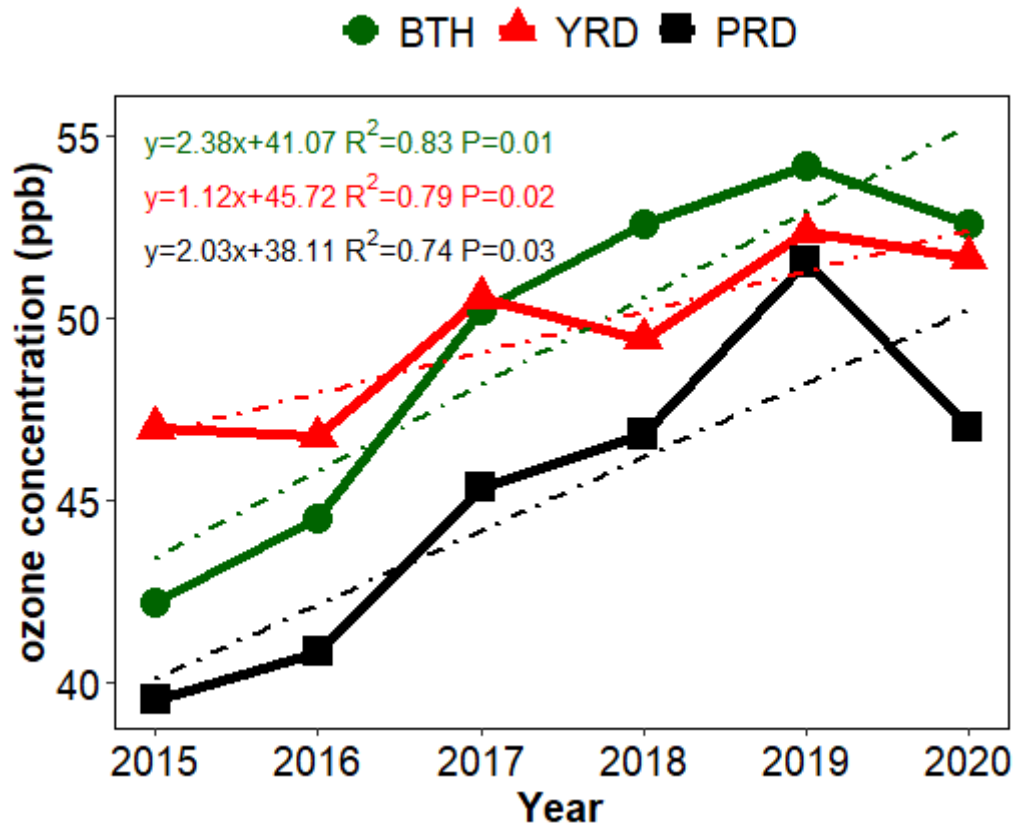
Figure 1: Annual mean concentrations of maximum daily 8-hour average O₃ in BTH (green), YRD (red) and PRD (black).
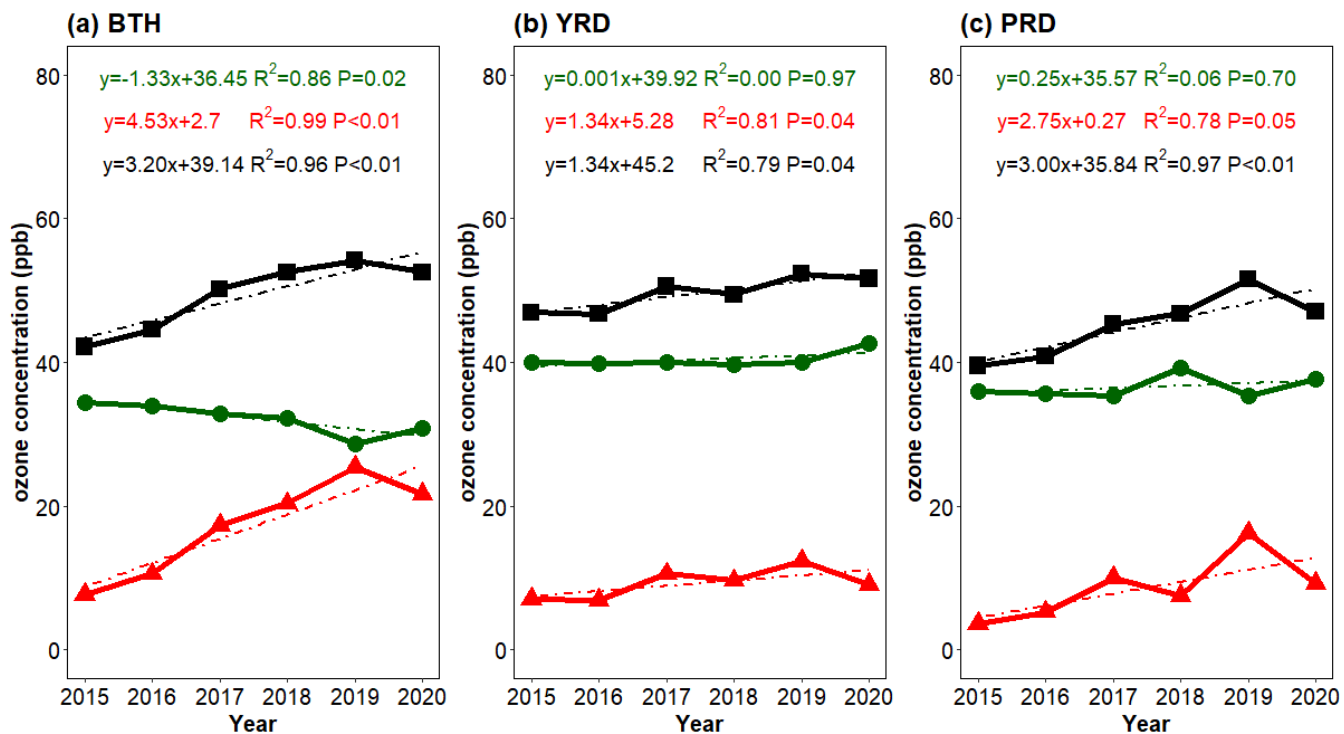
Figure 2: Contributions from the O₃-exceeding days (red) and non-O₃-exceeding days (green) to the annual mean concentration of maximum daily 8-hour average O₃ (black) in BTH (a), YRD (b) and PRD (c).
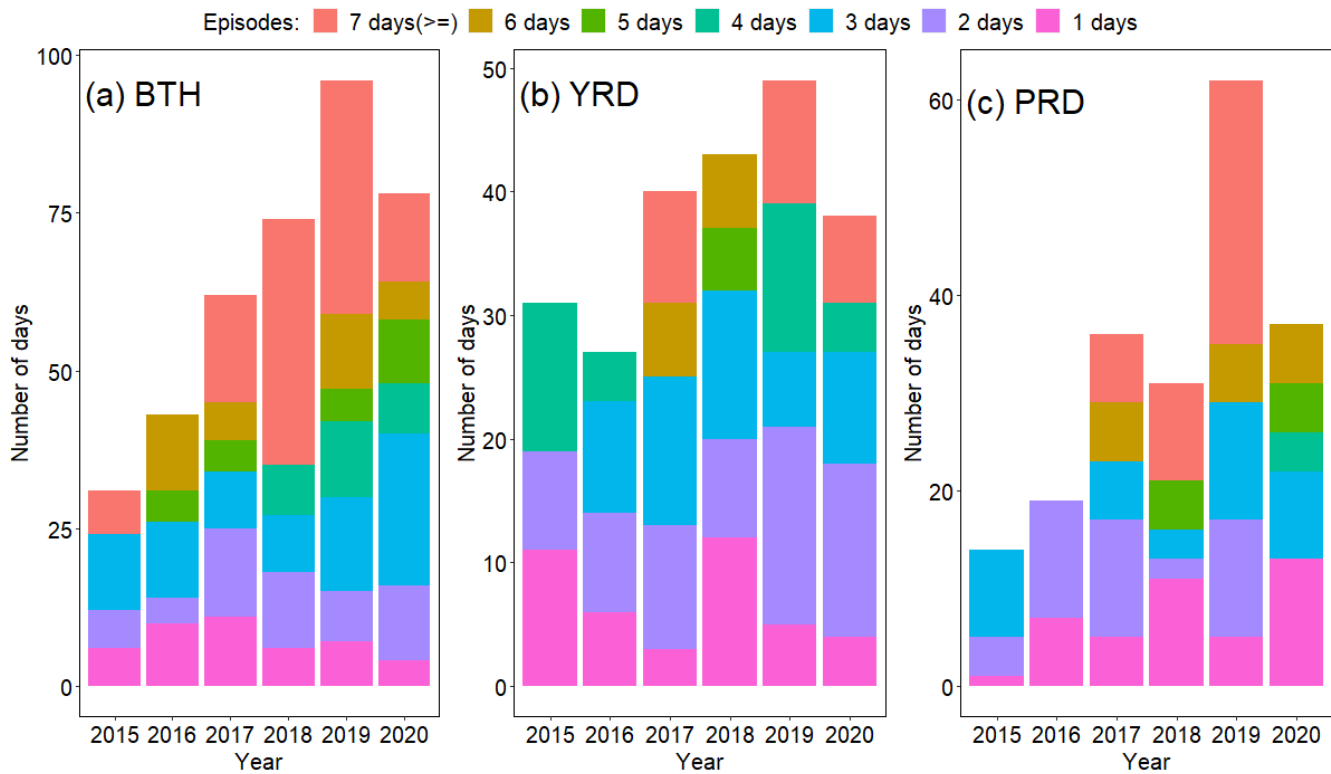
Figure 3: Annual numbers of various consecutive O$_3$-exceeding days in BTH (a), YRD (b) and PRD (c). Individual colors denote different numbers of consecutive O$_3$-exceeding days.
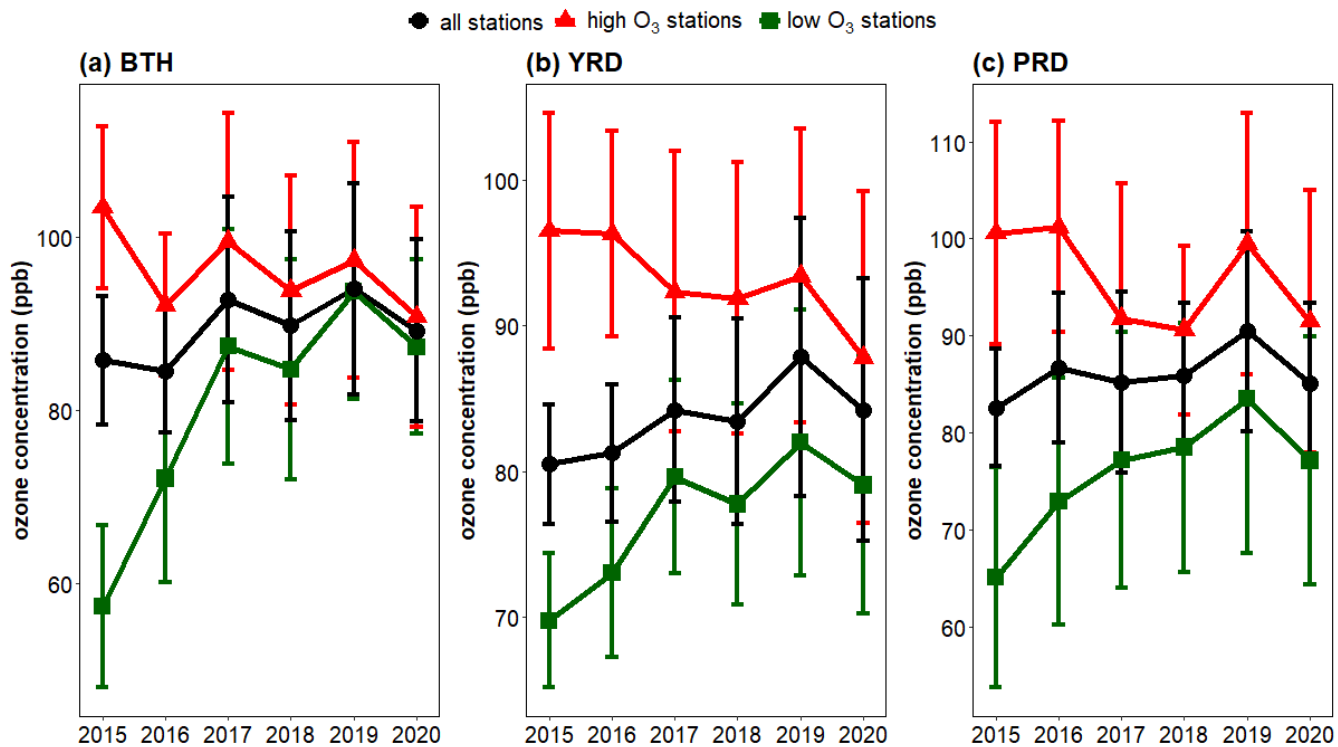
640 Figure 4: Annual mean concentrations (2015-2020) of maximum daily 8-hour average O_3 during O_3-exceeding days for all stations (black), high O_3 stations (red) and low O_3 stations (green) in BTH (a), YRD (b) and PRD (c).
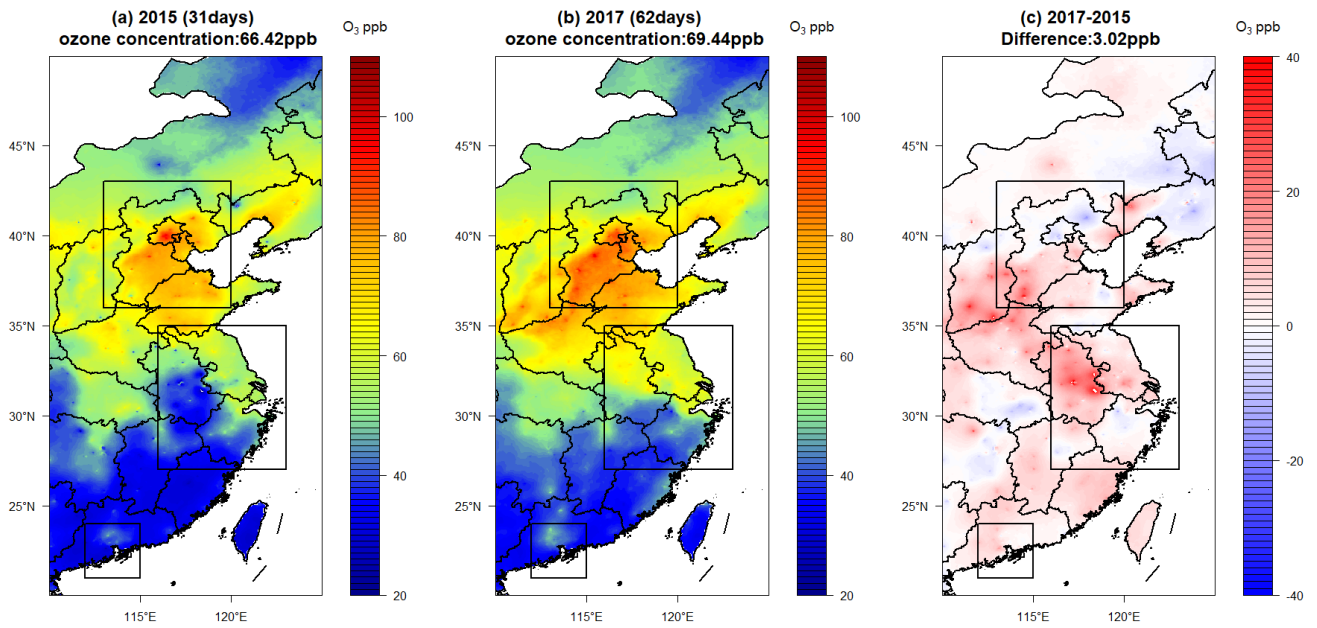
Figure 5: Spatial distribution of annual mean concentrations of maximum daily 8-hour average O_3 for O_3-exceeding days in BTH in 2015 (a), 2017 (b) and their difference (2017 - 2015) (c). The top, middle and bottom rectangle boxes denote BTH, YRD and PRD districts, respectively. The number inside the parenthesis behind 2015 or 2017 denotes the number of O_3-exceeding days.
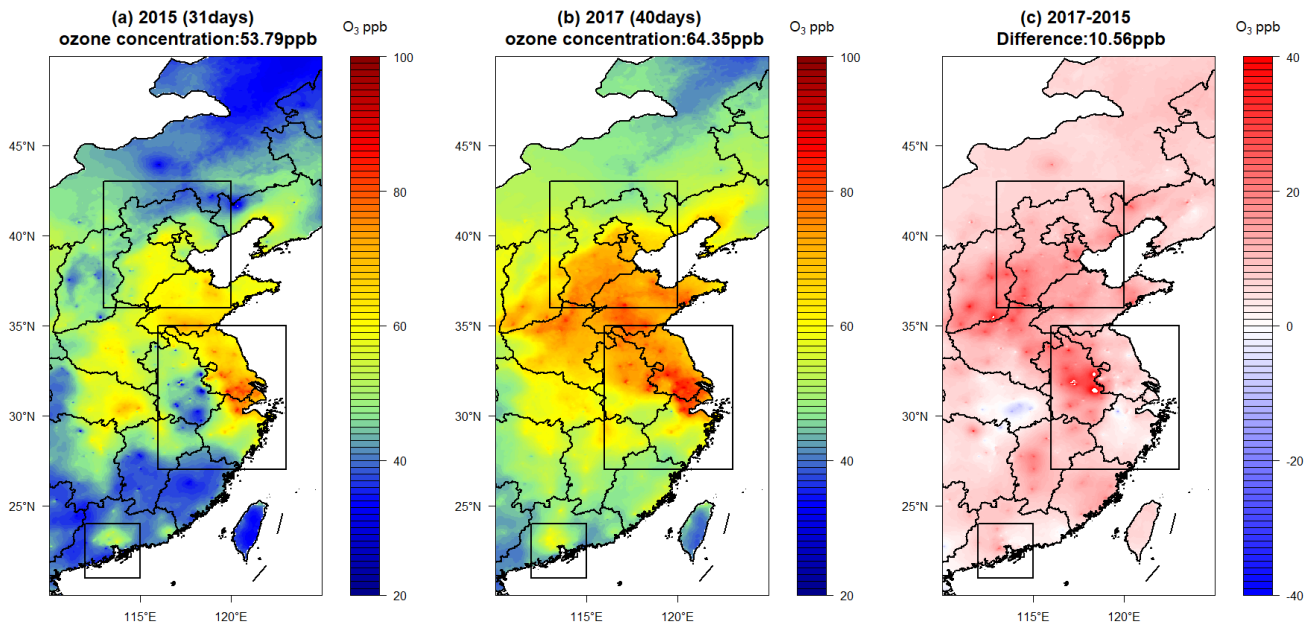
Figure 6: Spatial distribution of annual mean concentrations of maximum daily 8-hour average O₃ for O₃-exceeding days in YRD in 2015 (a), 2017 (b) and their difference (2017 - 2015) (c). The top, middle and bottom rectangle boxes denote BTH, YRD and PRD districts, respectively. The number inside the parenthesis behind 2015 or 2017 denotes the number of O₃-exceeding days.
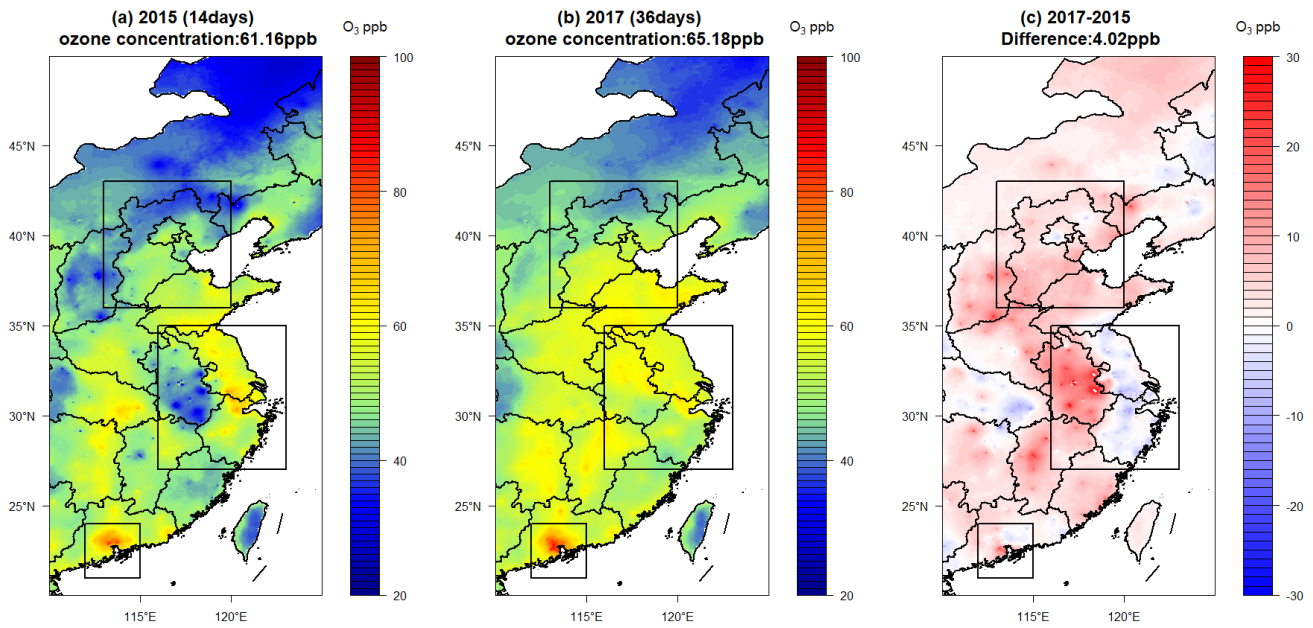
650

Figure 7: Spatial distribution of annual mean concentrations of maximum daily 8-hour average O₃ for O₃-exceeding days in PRD in 2015 (a), 2017 (b) and their difference (2017 - 2015) (c). The top, middle and bottom rectangle boxes denote BTH, YRD and PRD districts, respectively. The number inside the parenthesis behind 2015 or 2017 denotes the number of O₃-exceeding days.
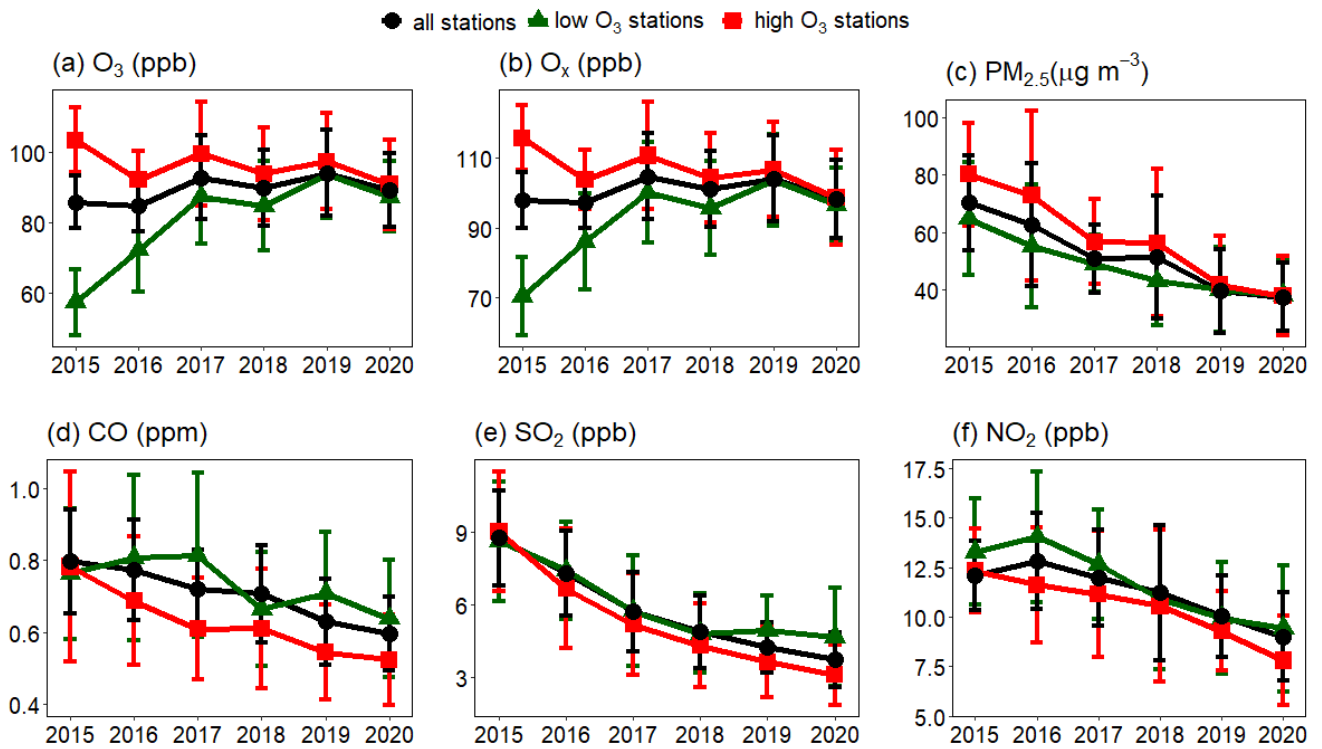
655   **Figure 8: Annual mean concentrations of maximum daily 8-hour average O₃ in BTH during O₃-exceeding days for all stations (black), high O₃ stations (red) and low O₃ stations (green) (a), same as (a) but for Ox (b), PM2.5 (c), CO (d), SO2 (e), NO2 (f).**
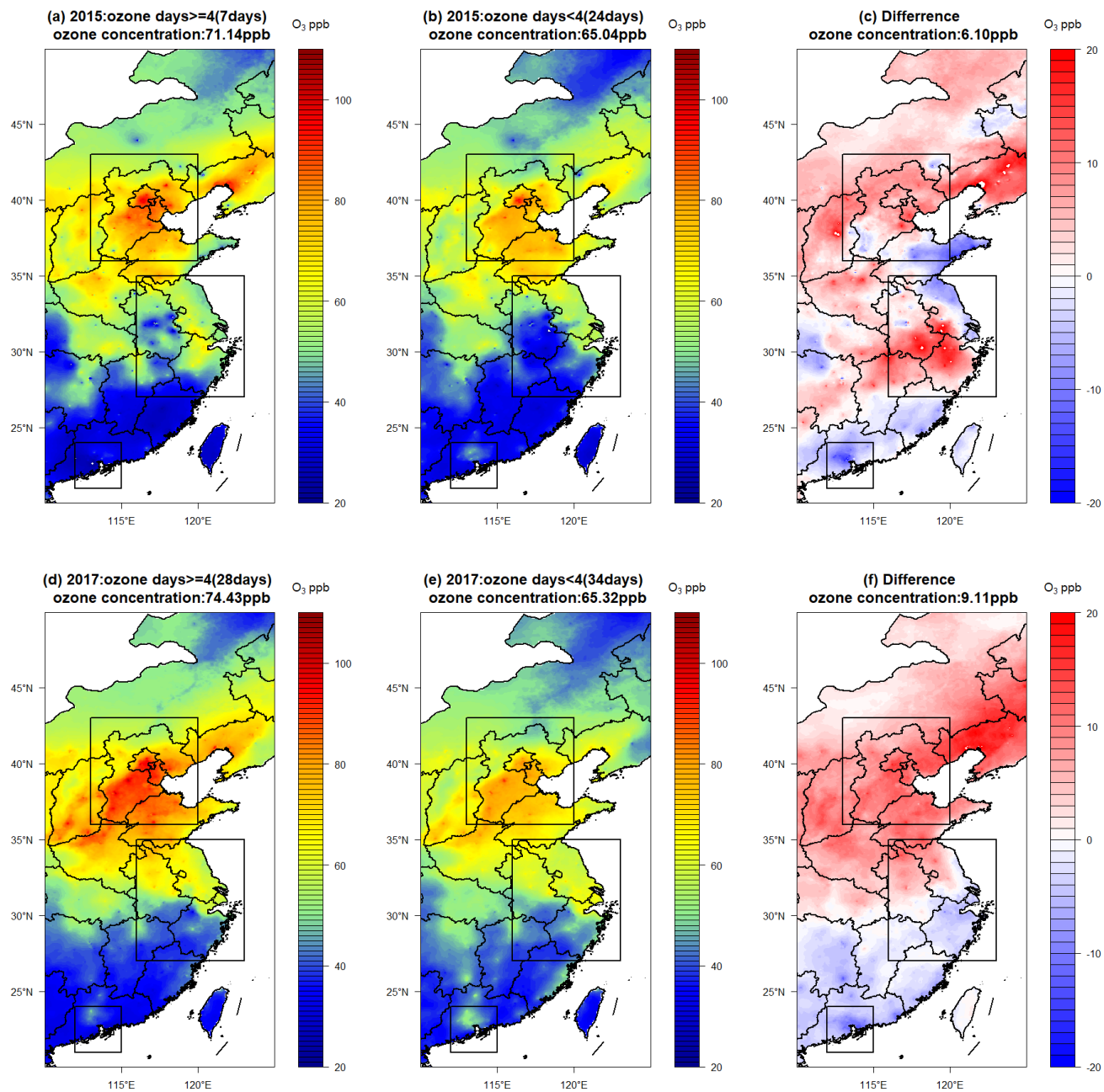
Figure 9: Spatial distribution of daily mean MDA8 O₃ of O₃-exceeding days in BTH for O₃ episodes with four or more consecutive O₃-exceeding days in 2015 (a), O₃ episodes with less than four consecutive O₃-exceeding days in 2015 (b), and (a minus b) (c); (d, e and f) are the same as (a, b and c), respectively, but for 2017.
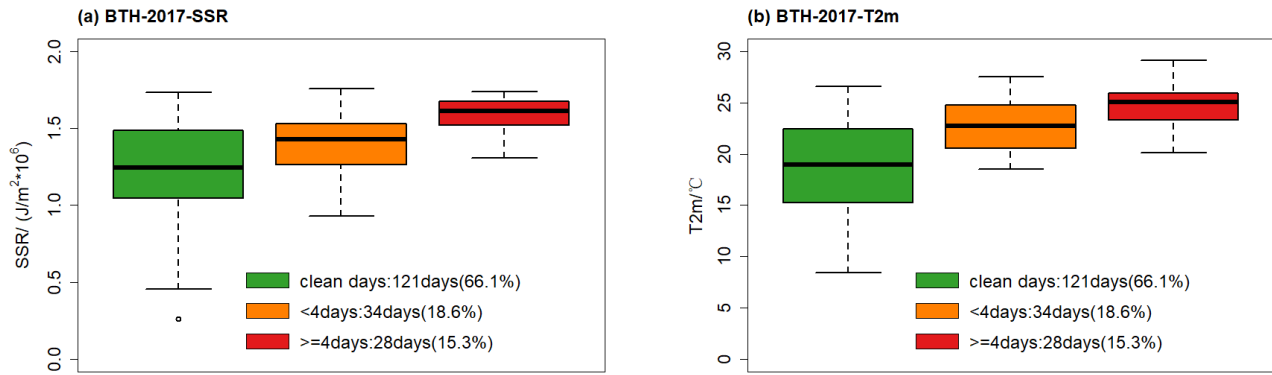
Figure 10: Surface solar radiation (SSR) (a) and temperature (T2m) (b) in BTH in April–September 2017 for four episodes with four or more consecutive O₃-exceeding days (red), clean days (non-O₃-exceeding days) (green) and O₃ episodes with less than four consecutive O₃-exceeding days (orange).
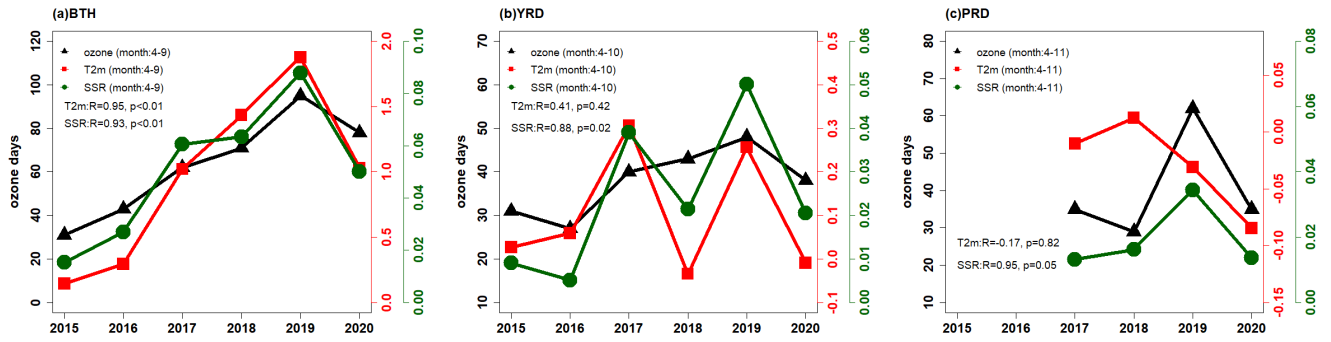
Figure 11: Correlations among annual O₃-exceeding days, surface solar radiation (SSR) and temperature (T2m) in BTH (a), YRD (b) and PRD (c).
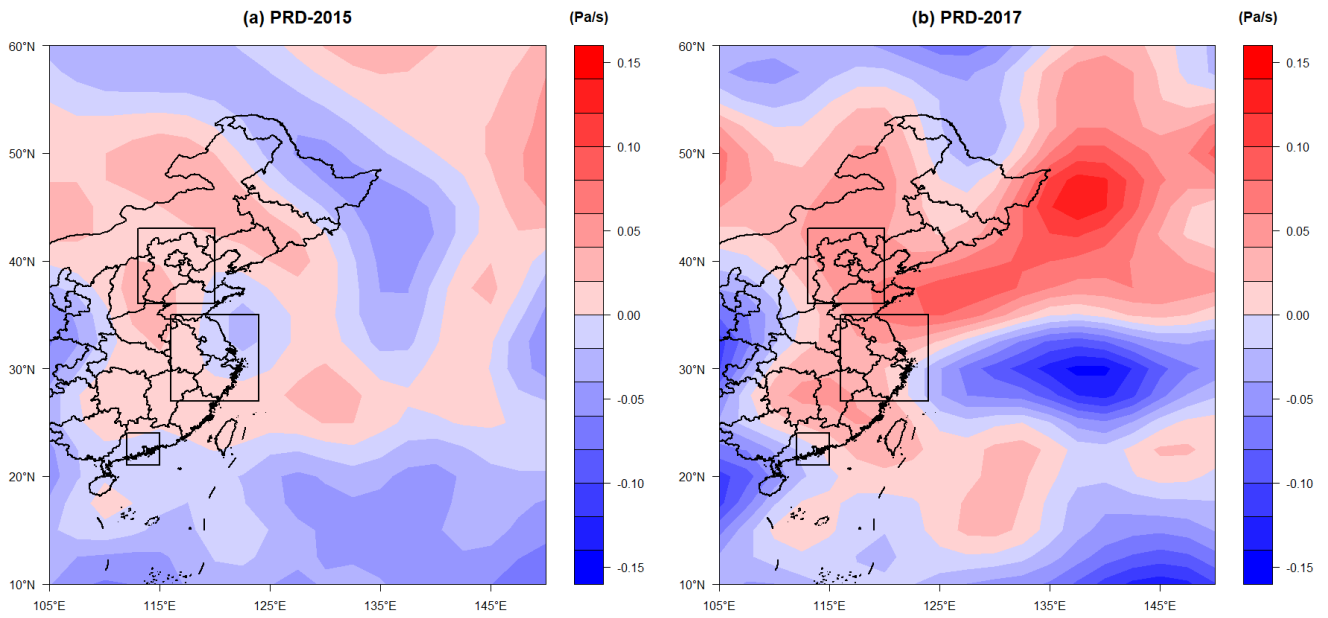
Figure 12: Mean vertical velocity at 850hPa during O₃-exceeding days in PRD in 2015 (a) and during episodes with four or more consecutive O₃-exceeding days in 2017 (b).
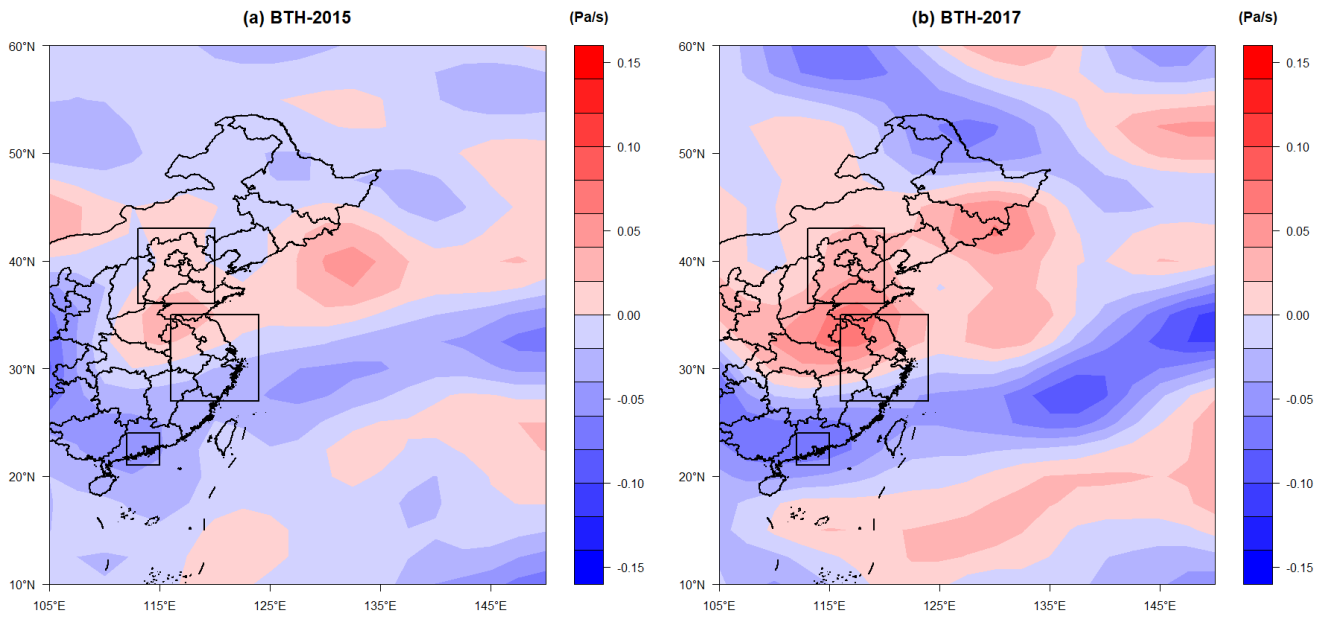
Figure 13: Mean vertical velocity at 850 hPa during O₃-exceeding days in BTH in 2015 (a) and during episodes with four or more consecutive O3-exceeding days in 2017 (b).
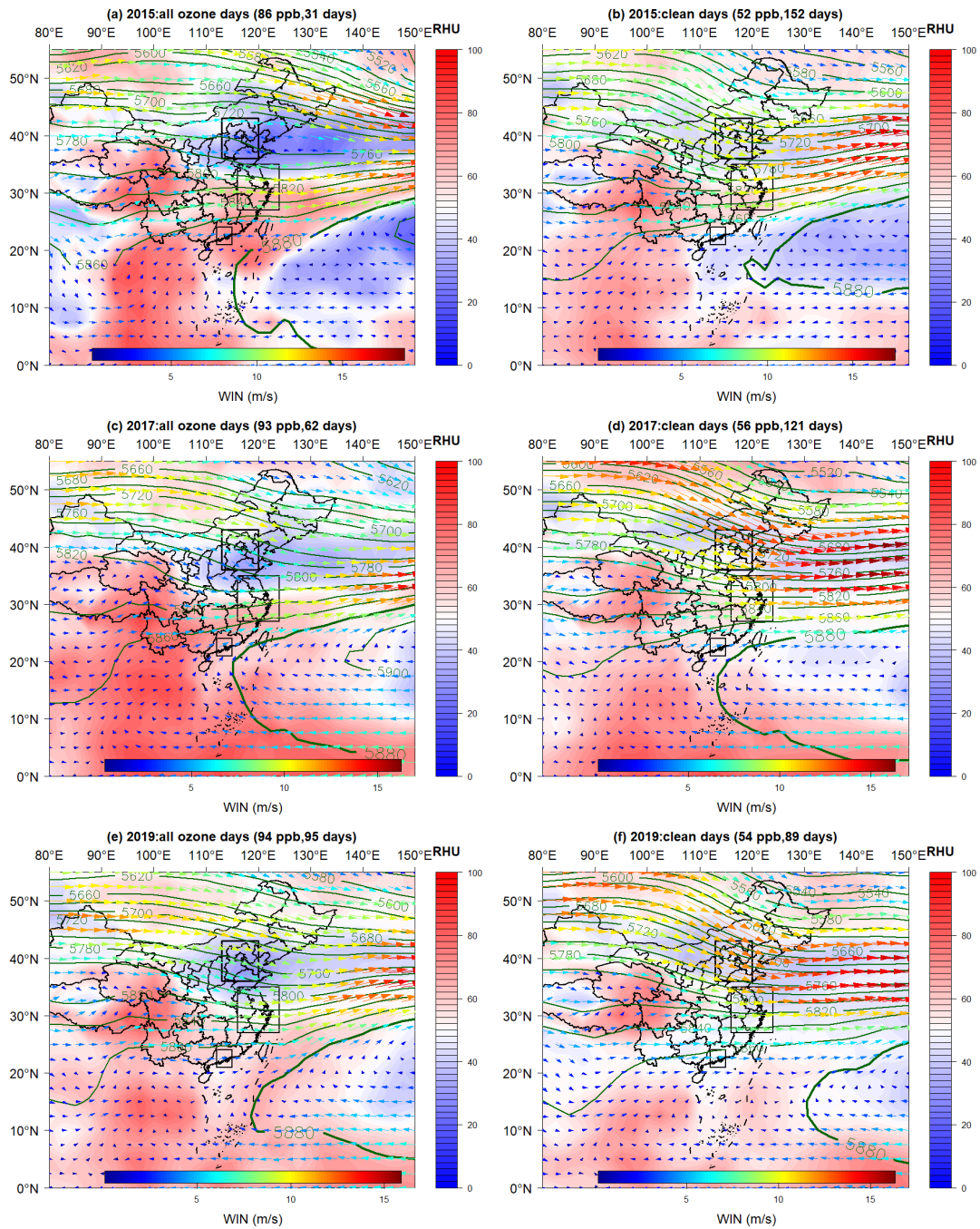
Figure 14: Composite 500 hPa geopotential height contours, humidity and winds in BTH in April-September for O$_3$-exceeding days in 2015 (a), clean days in 2015 (b), O$_3$-exceeding days in 2017 (c), clean days in 2017 (d), O$_3$-exceeding days in 2019 (e) and clean days in 2019 (f).
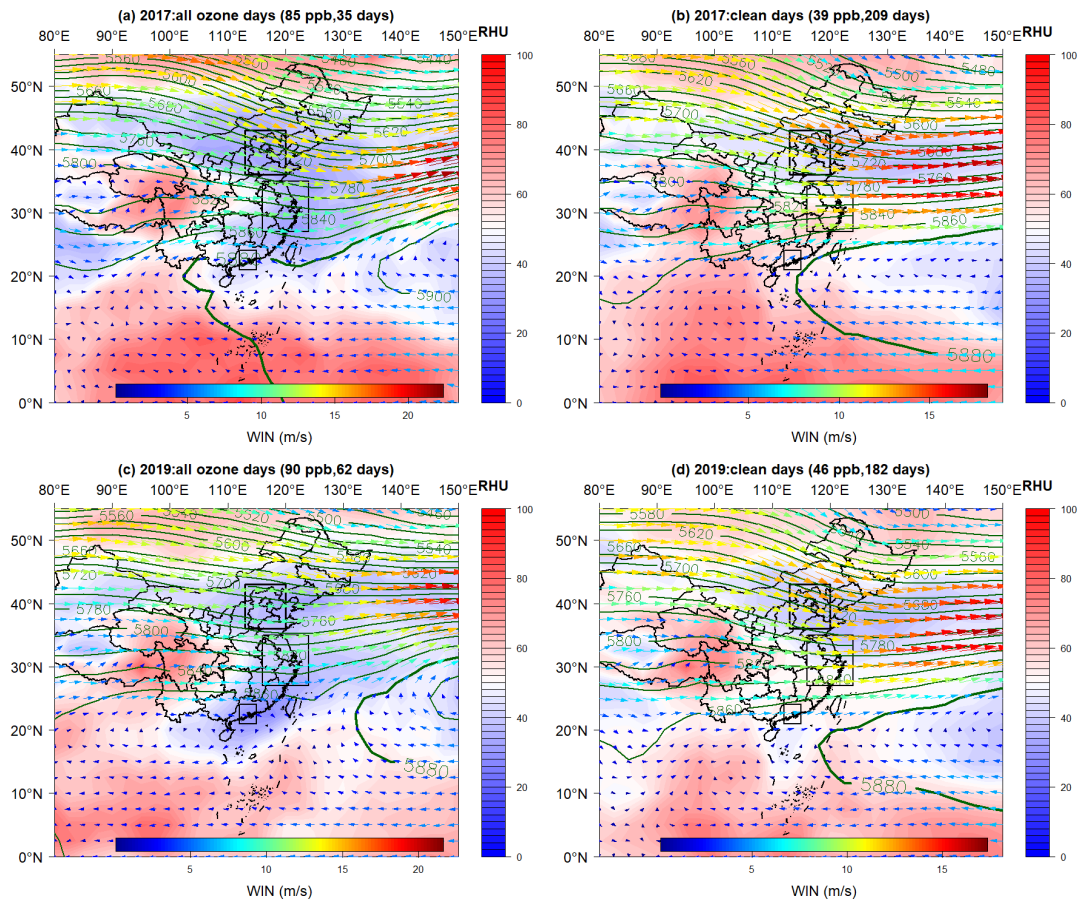
Figure 15: Composite 500 hPa geopotential height contours, humidity and winds in PRD in April-November for O₃-exceeding days in 2017 (a), clean days in 2017 (b), O₃-exceeding days in 2019 (c), clean days in 2019 (d).
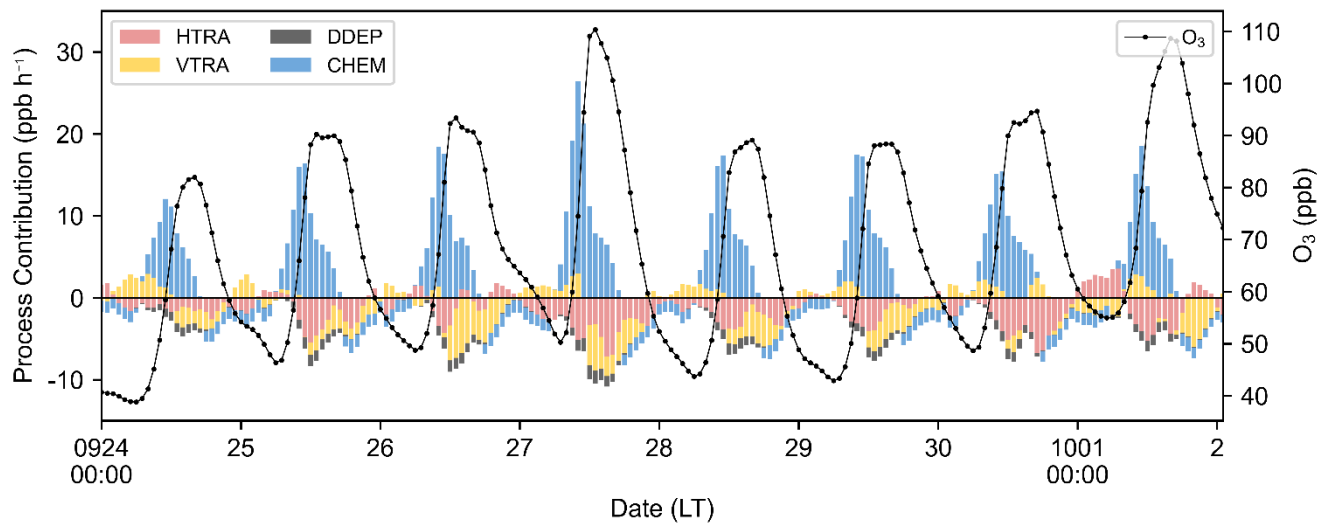
Figure 16: Time series of individual processes contributing to O₃ budget in PRD calculated by the WRF-CMAQ model for the O₃ episode of September 24–October 1, 2019. The black line (O₃) represents the averaged O₃ concentrations in the layers below 1260m. Where DDEP denotes dry deposition, CHEM denotes chemical processes, HTRA denotes the horizontal transport and VTRA denotes the vertical transport.